Perturbative QCD and beyond: azimuthal angle correlations in deuteron-deuteron scattering from Bose-Einstein correlations.

E. Gotsman[1,*] and E. Levin[1,2,†]

[1]*Department of Particle Physics, School of Physics and Astronomy, Raymond and Beverly Sackler Faculty of Exact Science, Tel Aviv University, Tel Aviv, 69978, Israel*
[2]*Departemento de Física, Universidad Técnica Federico Santa María, and Centro Científico-Tecnológico de Valparaíso, Avda. Espana 1680, Casilla 110-V, Valparaíso, Chile*

(Dated: November 8, 2016)

In this paper, we found within the framework of perturbative QCD, that in deuteron-deuteron scattering the Bose-Einstein correlations due to two parton showers production, induce azimuthal angle correlations, with three correlation lengths: the size of the deuteron (R_D), the proton radius (R_N), and the size of the BFKL Pomeron which, is closely related to the saturation momentum ($R_c \sim 1/Q_s$). These correlations are independent of the values of rapidities of the produced gluons (long range rapidity correlations), for large rapidities ($\bar{\alpha}_S|y_1 - y_2| \geq 1$), and have no symmetry with respect to $\phi \to \pi - \phi$ ($\boldsymbol{p}_{T1} \to -\boldsymbol{p}_{T1}$). Therefore, they give rise to v_n for all values of n, not only even values. The contributions with the correlation length R_D and R_N crucially depend on the non-perturbative contributions, and to obtain estimates of their values, requiries a lot of modeling, while the correlations with $R_c \sim 1/Q_s$ have a perturbative QCD origin, and can be estimated in the Color Glass Condensate (CGC) approach.

PACS numbers: 12.38.-t,24.85.+p,25.75.-q

arXiv:1611.01653v1 [hep-ph] 5 Nov 2016

I. INTRODUCTION

In this paper we continue to resurrect the old ideas of Gribov Pomeron Calculus, that the Bose -Einstein correlations lead to strong azimuthal angle correlations[1], which do not depend on the rapidity difference between measured hadrons (large range rapidity (LRR) correlations). In the framework of QCD, these azimuthal correlations stem from the production of two patron showers, and have been re-discovered in Refs.[2, 3]. In Ref.[4] it was demonstrated that Bose–Einstein correlations generate v_n with even and odd n, with values which are close to the experimental values [5–15].

The goal of this paper is to show that the Bose–Einstein correlations that have been discussed in Refs.[1, 4], arise naturally in the perturbative QCD approach, together with ones that have been considered in Refs.[2, 3]. We believe that the qualitative difference between these two approaches originates from different sources of the Bose-Einstein correlations: the two parton shower production in Refs.[1, 4] and one parton shower for Refs.[2, 3].

We consider here the azimuthal correlations for deuteron-deuteron scattering at high energy. It is well known[16], (see also Refs. [17]) that Bose-Einstein correlations provide a possibility to measure the volume of interaction or, in other words, the typical sizes of the interaction. Indeed, the general formula for the Bose-Einstein correlations [16, 17] takes the form

$$\frac{d^2\sigma}{dy_1\, dy_2 d^2p_{T1} d^2p_{T2}}\,(\text{identical gluons}) \;\propto\; \Big\langle 1 \;+\; e^{ir_\mu Q_\mu}\Big\rangle \tag{1}$$

where averaging $\langle \dots \rangle$ includes the integration over $r_\mu = r_{1,\mu} - r_{2,\mu}$. For the case of $y_1 = y_2$, $Q_\mu = p_{1,\mu} - p_{2,\mu}$ simplifies to $\boldsymbol{Q} \equiv \boldsymbol{p}_{T,12} = \boldsymbol{p}_{T1} - \boldsymbol{p}_{T2}$,

One can see that Eq. (1) allows us to measure the typical r_μ for the interaction. For deuteron-deuteron scattering we expect several typical r: the size of the deuteron R_D, the nucleon size R_N, and the typical size, related to the saturation scale ($r_{\rm sat} = 1/Q_s$, where Q_s denotes the saturation scale[18]). In our calculation we hope to see the appearance of these scales.

It is well known, that the total cross section for the deuteron-deuteron scattering can be written in the form: $\sigma_{DD} = 4\sigma_{NN} - \Delta\sigma_{DD}$, where $\Delta\sigma_{DD}$ is the Glauber correction term[19] which is proportional to $1/R_D^2$, while σ_{NN} denotes the total cross section of the nucleon-nucleon interaction. Intuition, suggests that the correlation radius of the order of R_D, stems from the production due to the Glauber correction term (see Fig. 1)

The production of two gluon are shown in Fig. 1-a and Fig. 1-b, where interference in the case of the generated identical gluon leads to the correlation function of Eq. (1). Generally speaking, the inclusive production of two gluons

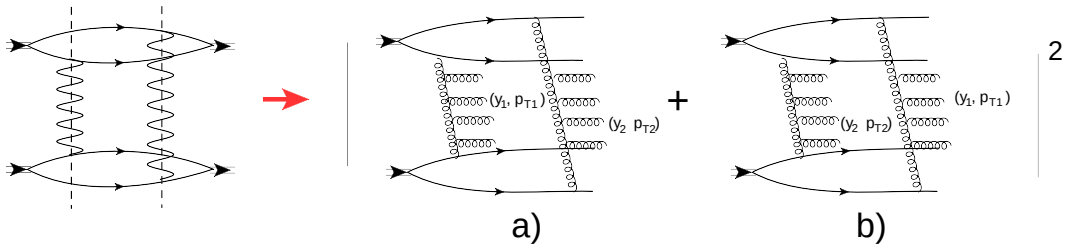

FIG. 1: The two parton showers production that contributes to the Glauber correction term for deuteron-deuteron scattering. The wavy lines describe the exchange of the BFKL Pomeron. Fig. 1-a and Fig. 1-b show two diagrams that can interfer for identical gluons. The dashed lines show the cut BFKL Pomeron [20].

with rapidities y_1 and y_2 and transverse momenta $\boldsymbol{p}_{T1}$ and $\boldsymbol{p}_{T2}$, takes the form

$$\frac{d^2\sigma}{dy_1\,dy_2 d^2p_{T1}d^2p_{T2}}\,(\text{identical gluons}) \;= \tag{2}$$
$$\frac{d^2\sigma}{dy_1\,dy_2 d^2p_{T1}d^2p_{T2}}\,(\text{different gluons})\left(\underbrace{1}_{\text{squared of diagrams}} + \underbrace{C\,(R_c|\boldsymbol{p}_{T1}-\boldsymbol{p}_{T2}|)}_{\text{interference diagram}}\right)$$

In Eq. (2) R_c denotes the correlation radius (correlation length), and in the form of the correlation function, we anticipate that the production of two parton showers leads to the double inclusive cross section, that does not depend on rapidities y_1 and y_2.

II. BORN APPROXIMATION

A. Bose-Einstein correlation function with radius $\propto$ R_D

The simplest contribution in the Born approximation of perturbative QCD is shown in Fig. 2. The second diagram describes the interference between two parton showers, shown in Fig. 1-b.

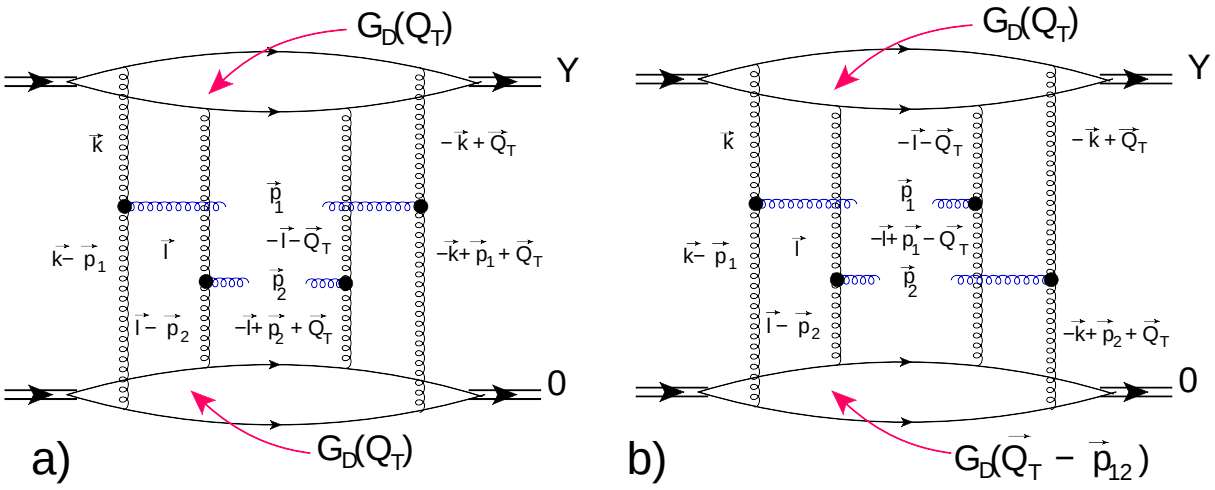

FIG. 2: The double inclusive production of two gluons with rapidities y_1 and y_2 and transverse momenta $\boldsymbol{p}_{T1}$ and $\boldsymbol{p}_{T2}$, in the Born Approximation of perturbative QCD. The interference diagram of Fig. 2-b gives the correlation function $C\,(R_D|\boldsymbol{p}_{T1}-\boldsymbol{p}_{T2}|)$ of Eq. (2). The solid lines denote nucleons in the deuterons, which are specified by double lines

The analytical expressions take the following forms. For the diagram of Fig. 2-a we have

$$\frac{d^2\sigma}{dy_1\,dy_2 d^2p_{T1} d^2p_{T2}}\,(Fig.\ 2-a)\ \propto\ \int d^2Q_T G_D^2\,(Q_T)$$
$$\times\ \int d^2k_t\,d^2l_T \left(\frac{I_P\,(\boldsymbol{k}_T,-\boldsymbol{k}_T+\boldsymbol{Q}_T)}{\boldsymbol{k}_T^2\ (\boldsymbol{k}-\boldsymbol{p}_1)_T^2}\Gamma_\mu\,(\boldsymbol{k}_T,\boldsymbol{p}_{T1})\ \Gamma_\mu\,(-\boldsymbol{k}_T+\boldsymbol{Q}_T,\boldsymbol{p}_{T1})\ \frac{I_P\,(\boldsymbol{k}_T-\boldsymbol{p}_{T1},-\boldsymbol{k}_T+\boldsymbol{p}_{T1}+\boldsymbol{Q}_T)}{(-\boldsymbol{k}+\boldsymbol{Q})_T^2\ (-\boldsymbol{k}+\boldsymbol{p}_1+\boldsymbol{Q})_T^2}\right)$$
$$\times\ \left(\frac{I_P\,(\boldsymbol{l}_T,-\boldsymbol{l}_T-\boldsymbol{Q}_T)}{\boldsymbol{l}_T^2\ (\boldsymbol{l}-\boldsymbol{p}_2)_T^2}\Gamma_\nu\,(\boldsymbol{l}_T,\boldsymbol{p}_{T2})\ \Gamma_\nu\,(-\boldsymbol{l}_T-\boldsymbol{Q}_T,\boldsymbol{p}_{T2})\ \frac{I_P\,(\boldsymbol{l}_T-\boldsymbol{p}_{T2},-\boldsymbol{l}_T+\boldsymbol{p}_{T2}-\boldsymbol{Q}_T)}{(-\boldsymbol{l}-\boldsymbol{Q})_T^2\ (-\boldsymbol{l}+\boldsymbol{p}_2-\boldsymbol{Q})_T^2}\right) \tag{3}$$

The interference diagram of Fig. 2-b takes the following form

$$\frac{d^2\sigma}{dy_1\,dy_2 d^2p_{T1} d^2p_{T2}}\,(Fig.\ 2-b)\ \propto\ \int d^2Q_T G_D\,(Q_T)\ G_D\left(\boldsymbol{Q}_T\ +\ \boldsymbol{p}_{T,12}\right)$$
$$\times\ \int d^2k_T\,d^2l_T \left(\frac{I_P\,(\boldsymbol{k}_T,-\boldsymbol{k}_T+\boldsymbol{Q}_T)}{\boldsymbol{k}_T^2\ (\boldsymbol{k}-\boldsymbol{p}_1)_T^2}\Gamma_\mu\,(\boldsymbol{k}_T,\boldsymbol{p}_{T1})\ \Gamma_\mu\,(-\boldsymbol{l}_T-\boldsymbol{Q}_T,\boldsymbol{p}_{T1})\ \frac{I_P\,(\boldsymbol{k}_T-\boldsymbol{p}_{T1},-\boldsymbol{k}_T+\boldsymbol{p}_{T1}+\boldsymbol{Q}_T)}{(-\boldsymbol{l}-\boldsymbol{Q})_T^2\ (-\boldsymbol{l}+\boldsymbol{p}_1-\boldsymbol{Q})_T^2}\right)$$
$$\times\ \left(\frac{I_P\,(\boldsymbol{l}_T,-\boldsymbol{l}_T-\boldsymbol{Q}_T)}{\boldsymbol{l}_T^2\ (\boldsymbol{k}-\boldsymbol{p}_2)_T^2}\Gamma_\mu\,(\boldsymbol{l}_T,\boldsymbol{p}_{T2})\ \Gamma_\mu\,(-\boldsymbol{k}_T+\boldsymbol{Q}_T,\boldsymbol{p}_{T2})\ \frac{I_P\,(\boldsymbol{l}_T-\boldsymbol{p}_{T2},-\boldsymbol{l}_T+\boldsymbol{p}_{T2}-\boldsymbol{Q}_T)}{(-\boldsymbol{k}+\boldsymbol{Q})_T^2\ (-\boldsymbol{k}+\boldsymbol{p}_2+\boldsymbol{Q})_T^2}\right) \tag{4}$$

The Lipatov vertices Γ_μ have the form (see reference [18] for example):

$$\Gamma_\mu\,(k_T,p_{T1})\ =\ \frac{1}{p_{T1}^2}\left(k_T^2\,\boldsymbol{p}_{T1}\ -\ \boldsymbol{k}_T\,p_{T1}^2\right);\qquad \Gamma_\mu\,(k_{T1},p_{T2})\ =\ \frac{1}{p_{T2}^2}\left(k_{T1}^2\,\boldsymbol{p}_{T2}\ -\ \boldsymbol{k}_{T1}\,p_{T2}^2\right); \tag{5}$$

and

$$\Gamma_\mu\,(k_T,p_{T1})\ \Gamma_\mu\,(k_{T1},p_{T2})\ =\ \frac{k_{T1}^2\ (\boldsymbol{k}_T-\boldsymbol{p}_{T2})^2}{p_{T2}^2}\ +\ \frac{k_T^2\ (\boldsymbol{k}_{T1}-\boldsymbol{p}_{T1})^2}{p_{T1}^2}\ -\ Q_T^2\ -\ p_{T,12}^2\frac{k_T^2\,k_{T1}^2}{p_{T1}^2\,p_{T2}^2} \tag{6}$$

where $\boldsymbol{p}_{T,12}\ =\ \boldsymbol{p}_{T1}-\boldsymbol{p}_{T2}$ and $\boldsymbol{k}_{T1}=\boldsymbol{k}_T-\boldsymbol{Q}_T$. One can see from Eq. (6) that

$$\begin{aligned}\Gamma_\mu\,(k_T,p_{T1})\ \Gamma_\mu\,(k_{T1},p_{T2}) \quad &\xrightarrow{k_T\ll Q_T} \quad k_T^2\left(1+\mathcal{O}\left(\frac{Q}{p_{T1}};\frac{k_T}{p_{T1}}\right)\right)\\ \Gamma_\mu\,(k_T,p_{T1})\ \Gamma_\mu\,(k_{T1},p_{T2}) \quad &\xrightarrow{k_{T1}\ll Q_T} \quad k_{T1}^2\left(1+\mathcal{O}\left(\frac{Q}{p_{T2}};\frac{k_{T1}}{p_{T2}}\right)\right);\end{aligned} \tag{7}$$

$G_D\,(Q_T)$ is equal to

$$G_D\,(Q_T)\ =\ \int d^2r\,e^{i\boldsymbol{r}\cdot\boldsymbol{Q}_T}|\Psi_D\,(r)\,|^2 \tag{8}$$

where r denotes the distance between the proton and the neutron in the deuteron. The impact factors ($I_P\,(\boldsymbol{k}_T,-\boldsymbol{k}_T+\boldsymbol{Q}_T)$ and others in Eq. (3) and Eq. (4)), determine the interaction of two gluons with the nucleon, and their typical momenta are about $1/R_N$.

From Eq. (8) we can see that typical $Q_T\ \propto\ 1/R_D$, where R_D is the deuteron radius. In other words, Q_T (and $|\boldsymbol{Q}_T\ +\ \boldsymbol{p}_{T,12}|$ in Eq. (4)) turn out to be much smaller than the value of k_T and l_T, which are determined by the size of the nucleon (R_N) $k_T\approx l_T\sim 1/R_N\gg\ Q_T(|\boldsymbol{Q}_T\ +\ \boldsymbol{p}_{T,12}|)\sim 1/R_D$, through the impact factors I_P in Eq. (3) and Eq. (4). The reason is that $R_D\ \gg\ R_N$. Neglecting Q_T and $p_{T,12}$ in comparison with k_T and l_T, we can simplify Eq. (3) and Eq. (4) to the form

$$\frac{d^2\sigma}{dy_1\,dy_2 d^2p_{T1} d^2p_{T2}}\,(Fig.\ 2-a)\ +\ \frac{d^2\sigma}{dy_1\,dy_2 d^2p_{T1} d^2p_{T2}}\,(Fig.\ 2-b)\ \propto \tag{9}$$
$$\frac{1}{p_{T1}^2\,p_{T2}^2}\int d^2Q_T\left\{G_D^2\,(Q_T)\ +\ \frac{1}{2\,(N_c^2-1)}\,G_D\,(Q_T)\ G_D\left(\boldsymbol{Q}_T\ +\ \boldsymbol{p}_{T,12}\right)\right\}$$
$$\times\ \int d^2k_t\,d^2l_T\left(\frac{I_P\,(\boldsymbol{k}_T,-\boldsymbol{k}_T)\ I_P\,(\boldsymbol{k}_T-\boldsymbol{p}_{T1},-\boldsymbol{k}_T+\boldsymbol{p}_{T1})}{\boldsymbol{k}_T^2\ (\boldsymbol{k}-\boldsymbol{p}_1)_T^2}\right)\ \times\ \left(\frac{I_P\,(\boldsymbol{l}_T,-\boldsymbol{l}_T)\ I_P\,(\boldsymbol{l}_T-\boldsymbol{p}_{T2},-\boldsymbol{l}_T+\boldsymbol{p}_{T2})}{\boldsymbol{l}_T^2\ (\boldsymbol{l}-\boldsymbol{p}_2)_T^2}\right)$$

In Eq. (9) we consider $p_1 = p_2$ for the expressions in $\Big(\dots\Big)$. Note, that the interference diagram of Fig. 2-b contributes when the polarizations of the produced gluons are the same, this fact is reflected in Eq. (4) by the same indices of Lipatov vertices. In Eq. (9) we replace

$$\begin{aligned}
&\Gamma_\mu\left(\boldsymbol{k}_T,\boldsymbol{p}_{T1}\right)\Gamma_\mu\left(-\boldsymbol{l}_T-\boldsymbol{Q}_T,\boldsymbol{p}_{T1}\right)\Gamma_\mu\left(\boldsymbol{l}_T,\boldsymbol{p}_{T2}\right)\Gamma_\mu\left(-\boldsymbol{k}_T+\boldsymbol{Q}_T,\boldsymbol{p}_{T2}\right)\\
&\qquad\to\quad \frac{1}{2}\Gamma_\mu\left(\boldsymbol{k}_T,\boldsymbol{p}_{T1}\right)\Gamma_\mu\left(-\boldsymbol{k}_T+\boldsymbol{Q}_T,\boldsymbol{p}_{T2}\right)\Gamma_\nu\left(\boldsymbol{l}_T,\boldsymbol{p}_{T2}\right)\Gamma_\nu\left(-\boldsymbol{l}_T-\boldsymbol{Q}_T,\boldsymbol{p}_{T1}\right) \qquad (10)\\
&\xrightarrow{Q_T,p_{T,12}\ll k_t,l_T}\quad \frac{1}{2}\Gamma_\mu\left(\boldsymbol{k}_T,\boldsymbol{p}_{T1}\right)\Gamma_\mu\left(-\boldsymbol{k}_T,\boldsymbol{p}_{T1}\right)\Gamma_\nu\left(\boldsymbol{l}_T,\boldsymbol{p}_{T2}\right)\Gamma_\nu\left(-\boldsymbol{l}_T,\boldsymbol{p}_{T2}\right)\\
&\qquad=\quad \frac{1}{2}\frac{1}{p_{T1}^2\,p_{T2}^2}\,k_T^2\;\left(\boldsymbol{k}-\boldsymbol{p}_1\right)_T^2\;l_T^2\;\left(\boldsymbol{l}-\boldsymbol{p}_2\right)_T^2 \qquad (11)
\end{aligned}$$

Factor $1/\left(N_c^2-1\right)$ in Eq. (9) reflects that identical gluons have the same colors (N_c is the number of colors).

Finally, the correlation function $C\left(R_c|\boldsymbol{p}_{T1}-\boldsymbol{p}_{T2}|\right)$ in Eq. (2) is equal to

$$C\left(R_D\,p_{T,12}\right)\;=\;\frac{1}{2\left(N_C^2-1\right)}\frac{\int d^2Q_T\,G_D\left(Q_T\right)\,G_D\left(|\boldsymbol{Q}_T+\boldsymbol{p}_{T,12}|\right)}{\int d^2Q_T\,G_D^2\left(Q_T\right)} \qquad (12)$$

B. Bose-Einstein correlation function with radius $\propto R_N$: Glauber corrections

In this subsection we show that the Glauber corrections due to interaction of one nucleon with two nucleons of the deuteron, shown in Fig. 3, lead to a correlation radius of the order of R_N. In the diagram of Fig. 3-a, Q_T is of the order of $1/R_D$ and, therefore, it is much smaller that the typical values of k_T and l_T, which are of the order of $1/R_N$. Hence, the contribution of this diagram is similar to Eq. (9): viz.

$$\begin{aligned}
&\frac{d^2\sigma}{dy_1\,dy_2 d^2p_{T1}d^2p_{T2}}\left(Fig.\;3-a\right)\;\propto\;\frac{1}{p_{T1}^2\,p_{T2}^2}\int d^2Q_T\,G_D\left(Q_T\right)\\
&\times\;\int d^2k_T\,d^2l_T\,I_P\left(\boldsymbol{k}_T,\boldsymbol{l}_T,-\boldsymbol{l}_T,-\boldsymbol{k}_T\right)\frac{I_P\left(\boldsymbol{k}_T-\boldsymbol{p}_{T1},-\boldsymbol{k}_T+\boldsymbol{p}_{T1}\right)\,I_P\left(\boldsymbol{l}_T-\boldsymbol{p}_{T2},-\boldsymbol{l}_T+\boldsymbol{p}_{T2}\right)}{\boldsymbol{k}_T^2\;\left(\boldsymbol{k}-\boldsymbol{p}_1\right)_T^2\;\boldsymbol{l}_T^2\;\left(\boldsymbol{l}-\boldsymbol{p}_2\right)_T^2}
\end{aligned}$$

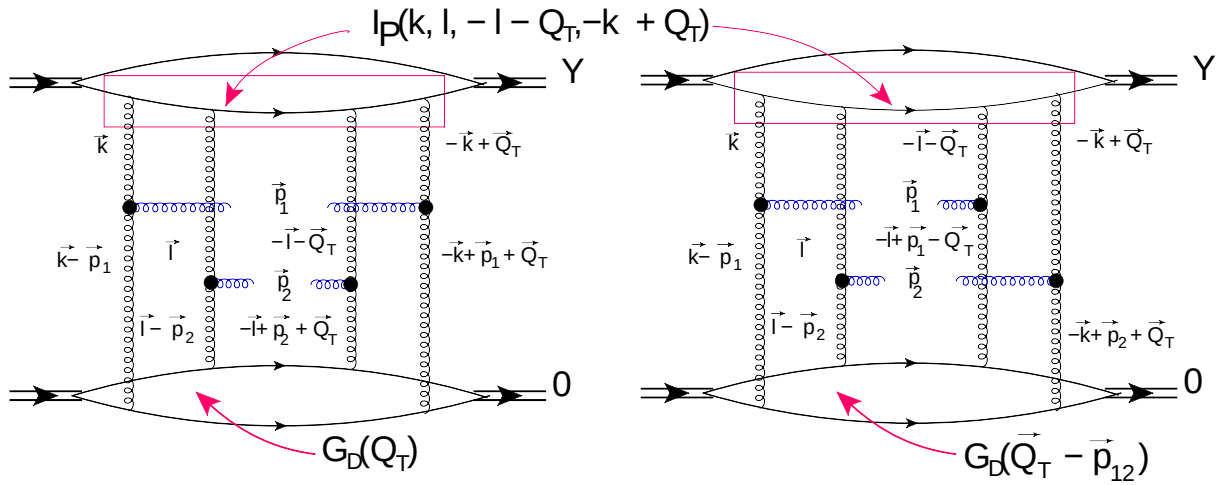

FIG. 3: The double inclusive production of two gluons with rapidities y_1 and y_2 and transverse momenta $\boldsymbol{p}_{T1}$ and $\boldsymbol{p}_{T2}$ in the Born Approximation of perturbative QCD. The interference diagram of Fig. 3-b yields the correlation function $C\left(R_N|\boldsymbol{p}_{T1}-\boldsymbol{p}_{T2}|\right)$ of Eq. (2). The solid lines denote nucleons in the deuterons, which are illustated by double lines

Unfortunately, we cannot treat the impact factors I_P theoretically in the case of nucleon. The phenomenological approach to I_P has been discussed in Refs.[4, 24], and we will return to this below. For the moment we replace the nucleon by the state of a heavy quark and antiquark (onium), to study the key features of the impact factors in the

framework of perturbative QCD (see Fig. 4). Introducing, the form factor of the onium in the form

$$F\left(Q_T\right) \;=\; \int d^2r\, e^{i\frac{1}{2}\boldsymbol{Q}_T\cdot\boldsymbol{r}}\left|\Psi_{\rm onium}\left(r\right)\right|^2 \tag{13}$$

we can express the impact factor in the form

$$I_P\left(\boldsymbol{k}_T,-\boldsymbol{k}_T+\boldsymbol{Q}_T\right) \;=\; F\left(\boldsymbol{Q}_T\right) \,-\, F\left(2\boldsymbol{k}_T+\boldsymbol{Q}_T\right); \tag{14}$$

$$\begin{aligned} I_P\left(\boldsymbol{k}_T,\boldsymbol{l}_T,-\boldsymbol{l}_T+\boldsymbol{Q}_T,-\boldsymbol{k}_T+\boldsymbol{Q}_T\right) \;=\; & 1 \,+\, F\left(2\boldsymbol{Q}_T\right) \,+\, F\left(2(\boldsymbol{k}_T+\boldsymbol{l}_T)\right) \,+\, F\left(2(\boldsymbol{k}_T-\boldsymbol{l}_T-\boldsymbol{Q}_T)\right) \\ & -\; F\left(2\boldsymbol{k}_T\right) \,-\, F\left(2(\boldsymbol{k}_T-\boldsymbol{Q}_T)\right) \,-\, F\left(2\boldsymbol{l}_T\right) \,-\, F\left(2(\boldsymbol{l}_T+\boldsymbol{Q}_T)\right) \end{aligned} \tag{15}$$

In Eq. (13) the impact factors are equal to

$$I_P\left(\boldsymbol{k}_T,-\boldsymbol{k}_T\right) \;=\; 1 \,-\, F\left(2\boldsymbol{k}_T\right); \qquad I_P\left(\boldsymbol{l}_T,-\boldsymbol{l}_T\right) \;=\; 1 \,-\, F\left(2\boldsymbol{l}_T\right); \tag{16}$$

$$I_P\left(\boldsymbol{k}_T,\boldsymbol{l}_T,-\boldsymbol{l}_T,-\boldsymbol{k}_T\right) \;=\; 2 \,+\, F\left(2(\boldsymbol{k}_T+\boldsymbol{l}_T)\right)+F\left(2(\boldsymbol{k}_T-\boldsymbol{l}_T)\right)-F\left(2\boldsymbol{k}_T\right) \,-\, F\left(2(\boldsymbol{k}_T)\right)-F\left(2\boldsymbol{l}_T\right)-F\left(2(\boldsymbol{l}_T)\right); \tag{17}$$

The integration over k_T and l_T lead to typical values of $k_T \sim 1/R_N$ and $l_T \sim 1/R_N$, and it does not generate azimuthal angle correlations. Indeed, this is clear from the following features of I_P from Eq. (17):

$$\begin{aligned} & R_N\, k_T \ll 1, R_N\, l_T \ll 1; \quad I_P\left(\boldsymbol{k}_T,\boldsymbol{l}_T,-\boldsymbol{l}_T,-\boldsymbol{k}_T\right) \;\propto\; k_T^2\, l_T^2; \\ & R_N\, k_T \ll 1, R_N\, l_T \gg 1; \quad I_P\left(\boldsymbol{k}_T,\boldsymbol{l}_T,-\boldsymbol{l}_T,-\boldsymbol{k}_T\right) \;\propto\; k_T^2; \\ & R_N\, k_T \gg 1, R_N\, l_T \ll 1; \quad I_P\left(\boldsymbol{k}_T,\boldsymbol{l}_T,-\boldsymbol{l}_T,-\boldsymbol{k}_T\right) \;\propto\; l_T^2; \\ & R_N\, k_T \gg 1, R_N\, l_T \gg 1; \quad I_P\left(\boldsymbol{k}_T,\boldsymbol{l}_T,-\boldsymbol{l}_T,-\boldsymbol{k}_T\right) \;\propto\; 1; \end{aligned} \tag{18}$$

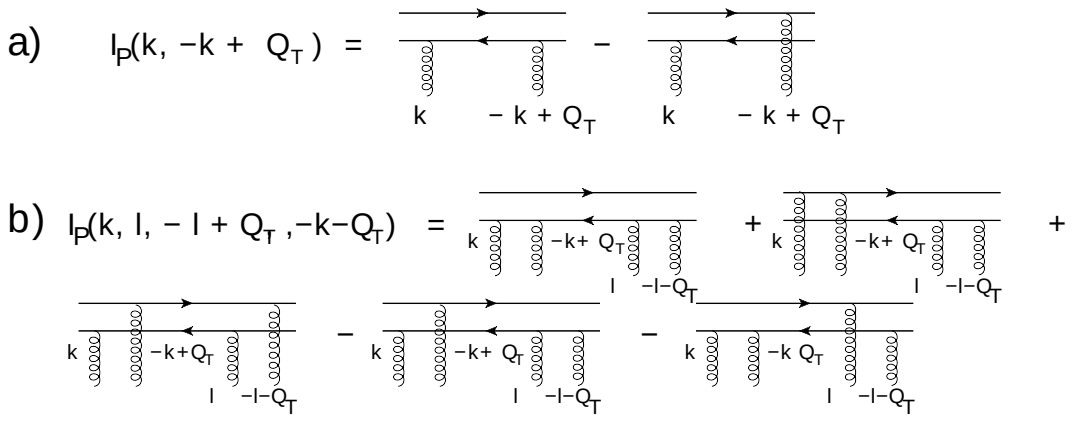

FIG. 4: The impact factors for onium for $R_N k_T > 1$, $R_N l_T > 1$ and $R_N Q_T > 1$

In the diagram of Fig. 3-b one can see that $G_D\left(\boldsymbol{Q}_T-\boldsymbol{p}_{12}\right)$ regulates that $|\boldsymbol{Q}_T-\boldsymbol{p}_{12}|$ is of the order of $1/R_D$. This means that we can put $\boldsymbol{Q}_T=\boldsymbol{p}_{12}$ in all parts of diagrams, since the typical values of k_T and l_T are about $1/R_N \gg 1/R_D$. Therefore, the diagram of Fig. 3-b can be reduced to the form

$$\begin{aligned} & \frac{d^2\sigma}{dy_1\, dy_2 d^2p_{T1} d^2p_{T2}}\left(Fig.\ 3-b\right) \;\propto\; \frac{1}{p_{T1}^2\, p_{T2}^2}\int d^2Q_T G_D\left(\boldsymbol{Q}_T-\boldsymbol{p}_{12}\right) \\ & \times \int d^2k_T\, d^2l_T\, I_P\left(\boldsymbol{k}_T,\boldsymbol{l}_T,-\boldsymbol{l}_T-\boldsymbol{p}_{12},-\boldsymbol{k}_T+\boldsymbol{p}_{12}\right)\, I_P\left(\boldsymbol{k}_T-\boldsymbol{p}_{T1},-\boldsymbol{k}_T+\boldsymbol{p}_{T1}\right)\, I_P\left(\boldsymbol{l}_T-\boldsymbol{p}_{T2},-\boldsymbol{l}_T+\boldsymbol{p}_{T2}\right) \\ & \times \left\{\left(\frac{1}{\left(\boldsymbol{k}-\boldsymbol{p}_1\right)_T^2\,\left(\boldsymbol{l}+\boldsymbol{p}_{12}\right)_T^2}+\frac{1}{k_T^2\,\left(\boldsymbol{l}-\boldsymbol{p}_2\right)_T^2}\right)-\frac{\left(\boldsymbol{l}-\boldsymbol{k}+\boldsymbol{p}_{12}\right)_T^2\, p_{T,1}^2}{k_T^2\,\left(\boldsymbol{k}-\boldsymbol{p}_1\right)_T^2\,\left(\boldsymbol{l}-\boldsymbol{p}_2\right)_T^2\,\left(\boldsymbol{l}+\boldsymbol{p}_{12}\right)^2}\right\} \\ & \times \left\{\left(\frac{1}{\left(\boldsymbol{l}-\boldsymbol{p}_2\right)_T^2\,\left(\boldsymbol{k}-\boldsymbol{p}_{12}\right)_T^2}+\frac{1}{l_T^2\,\left(\boldsymbol{k}-\boldsymbol{p}_1\right)_T^2}\right)-\frac{\left(\boldsymbol{l}-\boldsymbol{k}+\boldsymbol{p}_{12}\right)_T^2\, p_{T,2}^2}{l_T^2\,\left(\boldsymbol{l}-\boldsymbol{p}_2\right)_T^2\,\left(\boldsymbol{k}-\boldsymbol{p}_1\right)_T^2\,\left(\boldsymbol{k}-\boldsymbol{p}_{12}\right)^2}\right\} \end{aligned} \tag{19}$$

The largest contributions to the integrals over k_T and l_T lead to the logarithmically large terms, which are proportional to $\ln\left(p_{T1}^2\, R_N^2\right)\, \ln\left(p_{T2}^2\, R_N^2\right)$. These contribution stems from the terms which are proportional to $1/\left(\left(\boldsymbol{k}-\boldsymbol{p}_1\right)_T^2\right)^2$, and

to $1/\left((\boldsymbol{l}-\boldsymbol{p}_2)_T^2\right)^2$. We consider the kinematic region in the integration over k_T and l_T, where $\boldsymbol{k}_T-\boldsymbol{p}_{T1}\equiv\boldsymbol{k}_1\to 0$ and $\boldsymbol{l}_T-\boldsymbol{p}_{T2}\equiv\boldsymbol{l}_2\to 0$. For small $k_1\ll p_{T2}$ and $l_2\ll p_{T1}$ the product of curly brackets is equal to

$$\frac{1}{p_{T1}^2}\left\{\frac{1}{k_1^2}+\frac{1}{l_1^2}-\frac{(\boldsymbol{k}_1-\boldsymbol{l}_2)^2}{k_1^2\,l_2^2}\right\}\frac{1}{p_{T2}^2}\left\{\frac{1}{k_1^2}+\frac{1}{l_1^2}-\frac{(\boldsymbol{k}_1-\boldsymbol{l}_2)^2}{k_1^2\,l_2^2}\right\}=\frac{4\,(\boldsymbol{k}_1\cdot\boldsymbol{l}_2)^2}{p_{T1}^2\,p_{T2}^2\,k_1^4\,l_2^4}\xrightarrow{\text{after integration over angle}}\frac{2}{p_{T1}^2\,p_{T2}^2\,k_1^2\,l_2^2} \tag{20}$$

For $R_N k_1\ll 1$, $I_P\left(\boldsymbol{k}_T-\boldsymbol{p}_{T1},-\boldsymbol{k}_T+\boldsymbol{p}_{T1}\right)\propto k_1^2$, and the integral over k_1 gives a small contribution of the order of $1/(R_N^2p_{T1}^2)$. Recall that we can use the perturbative QCD approach only if $R_Np_{T1}\gg 1$ and $R_Np_{T2}\gg 1$. Therefore, the main contribution occurs from the region of integration $(1/R_N^2)\ll k_1\ll p_{T2}$ and $(1/R_N^2)\ll l_1\ll p_{T1}$. Integration in this region leads to the contribution

$$\begin{aligned}\frac{d^2\sigma}{dy_1\,dy_2d^2p_{T1}d^2p_{T2}}\,(Fig.\ 3-b)\ &\propto\ \frac{1}{p_{T1}^4\,p_{T2}^4}\,\ln\left(p_{T1}^2R_N^2\right)\ln\left(p_{T2}^2R_N^2\right)\int d^2Q_T G_D\left(\boldsymbol{Q}_T-\boldsymbol{p}_{12}\right)\\ &\times\ I_P\left(\boldsymbol{p}_{T1},\boldsymbol{p}_{T2},-\boldsymbol{p}_{T1},-\boldsymbol{p}_{T2}\right)\end{aligned} \tag{21}$$

Therefore, from this kinematic region the correlations are determined by the impact factor. Using the impact factor given in Eq. (15), we see that

$$I_P\left(\boldsymbol{p}_{T1},\boldsymbol{p}_{T2},\boldsymbol{p}_{T1},\boldsymbol{p}_{T2}\right)\ =\ 2+F\left(2\left(\boldsymbol{p}_{T1}+\boldsymbol{p}_{T2}\right)\right)+F\left(2\boldsymbol{p}_{T,12}\right)-2F\left(2\boldsymbol{p}_{T1}\right)-2F\left(\boldsymbol{p}_{T2}\right) \tag{22}$$

This function is symmetric with respect to $\phi\to\pi-\phi$ ($\boldsymbol{p}_{T1}\to-\boldsymbol{p}_{T1}$), and with such an impact factor, the Born approximation produces only v_n with even n, as was noted in Ref.[2, 3]. However, this conclusion is based on the impact factor of Eq. (15). Eq. (22) shows that this impact factor leads to $p_{T,12}\sim 1/R_N$.

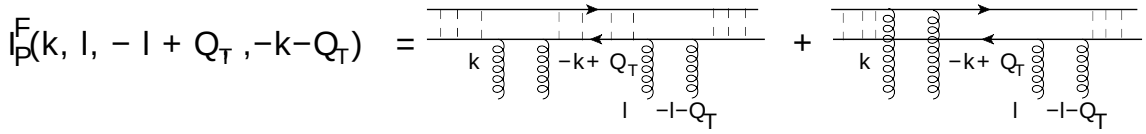

FIG. 5: The impact factors for onium for for $R_Nk_T>1$, $R_Nl_T>1$ and $R_NQ_T\le 1$. The dashed lines denote the Coulomb gluons that form the onium bound state.

Note that the simple expression of Eq. (15) (see Fig. 4) is written for sufficiently hard gluons. For small values of $Q_T=p_{T,12}$ we need to add the first diagram of Fig. 5, in which two gluons with large transverse momenta (about p_{T1} or p_{T2}) but small Q_T. The final expression for the impact factor takes the form

$$I_P^F\left(\boldsymbol{k}_T,\boldsymbol{l}_T,-\boldsymbol{l}_T+\boldsymbol{Q}_T,-\boldsymbol{k}_T+\boldsymbol{Q}_T\right)\ =\ I_P\left(\boldsymbol{k}_T,-\boldsymbol{k}_T+\boldsymbol{Q}_T\right)\,I_P\left(\boldsymbol{l}_T,-\boldsymbol{l}_T-\boldsymbol{Q}_T\right)\ +\ \underbrace{I_P\left(\boldsymbol{k}_T,\boldsymbol{l}_T,-\boldsymbol{l}_T+\boldsymbol{Q}_T,-\boldsymbol{k}_T+\boldsymbol{Q}_T\right)}_{\text{Eq. (15)}} \tag{23}$$

The first term in Eq. (23) generates the correlation function which is proportional to $F^2\left(2\boldsymbol{p}_{T,12}\right)$.

Summarizing, we see that the Born approximation of perturbative QCD, generates the correlation function which is determined by the impact factor of the nucleon, the typical correlation length is about R_N, and even for the unrealistic perturbative model of onium, this correlation function is not symmetric with respect to $\phi\to\pi-\phi$. We will consider below the more realistic case, in leading log approximation of perturbative QCD. However, we would like to stress now, that the correlation function stems from the large non-perturbative distances of the order of the nucleon size.

C. Bose-Einstein correlation function with radius $\propto$ R_N: nucleon-nucleon interaction

The correlations with $R_c=R_N$ are typical for the nucleon-nucleon interaction (see Fig. 6 for the Born approximation of perturbative QCD). However, we will consider them below for the general case of the production of two parton showers, since we prefer to use a more phenomenological and realistic approach for the impact factors I_P, than we

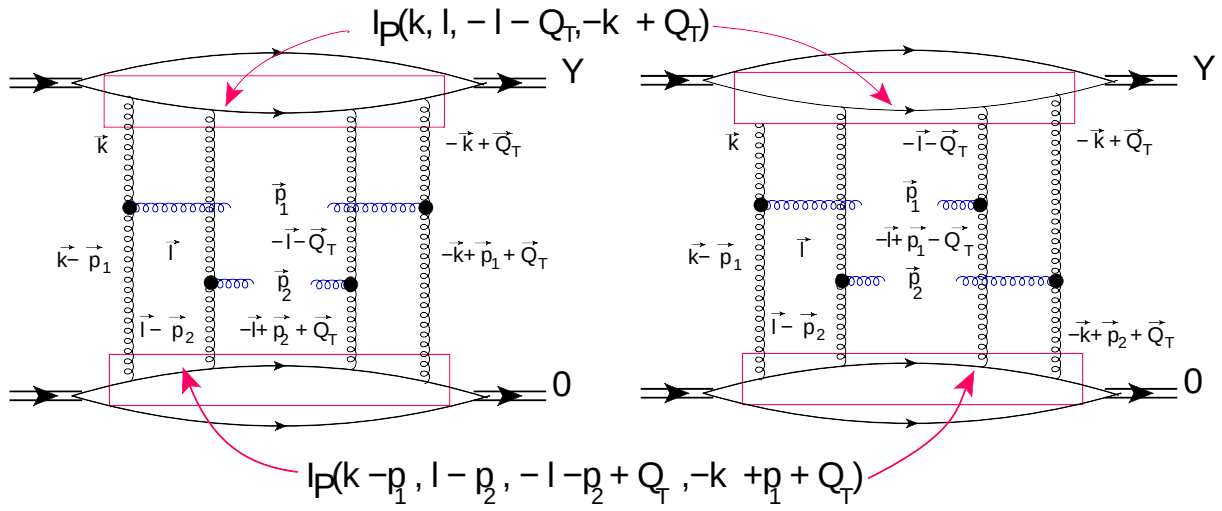

FIG. 6: The double inclusive production of two gluons with rapidities y_1 and y_2 and transverse momenta $\boldsymbol{p}_{T1}$ and $\boldsymbol{p}_{T2}$ in the Born Approximation of perturbative QCD for the nucleon-nucleon interaction. The interference diagram of Fig. 6-b yields the correlation function $C\left(R_D|\boldsymbol{p}_{T1} - \boldsymbol{p}_{T2}|\right)$ of Eq. (2). The solid lines denote nucleons in the deuterons, which are illustrated by double lines.

explored above, replacing the nucleon by the onium state.

III. PRODUCTION OF TWO PARTON SHOWERS

A. $R_c \propto R_D$

In this section we consider the general case of the production of two parton showers shown in Fig. 1. In the leading log approximation (LLA) of perturbative QCD, the structure of one parton shower is described by the BFKL Pomeron[21, 22]. In the leading log approximation of perturbative QCD the Born diagram of Fig. 2-a can be generalized

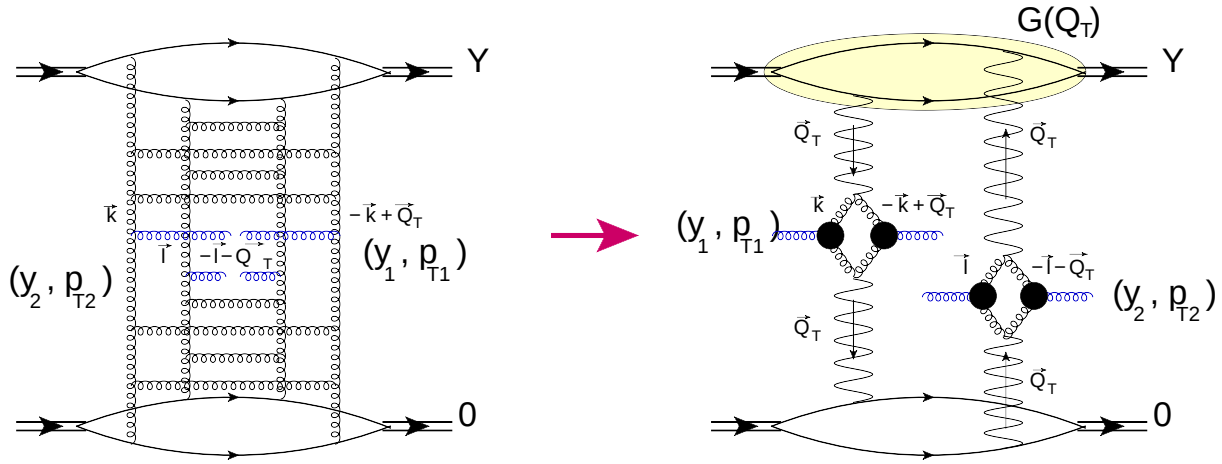

FIG. 7: The double inclusive production of two gluons with rapidities y_1 and y_2 and transverse momenta $\boldsymbol{p}_{T1}$ and $\boldsymbol{p}_{T2}$, for the exchange of two BFKL Pomerons which are denoted by wavy lines. This diagram is the LLA generalization of Fig. 2-a. The solid lines denote nucleons in the deuterons, which are indicated by double lines.

to Fig. 7. The contribution of this diagram can be written as follows

$$\frac{d^2\sigma}{dy_1\,dy_2 d^2p_{T1}d^2p_{T2}}\,(Fig.\ 7) \;=\; \left(\frac{2\pi\bar{\alpha}_S}{C_F}\right)^2 \frac{1}{p_{T,1}^2\,p_{T2}^2}\int d^2Q_T G_D^2\,(Q_T)$$
$$\times\;\left(\int d^2k_T\;\phi_G^N\,(Y-y_1;\boldsymbol{k}_T,-\boldsymbol{k}_T+\boldsymbol{Q}_T)\;\phi_G^N\,(y_1;\boldsymbol{k}_T-\boldsymbol{p}_{T1},-\boldsymbol{k}_T+\boldsymbol{p}_{T1}+\boldsymbol{Q}_T)\right)$$
$$\times\;\left(\int d^2l_T\;\phi_G^N\,(Y-y_2;\boldsymbol{l}_T,-\boldsymbol{l}_T-\boldsymbol{Q}_T)\;\phi_G^N\,(y_2;\boldsymbol{l}_T-\boldsymbol{p}_{T2},-\boldsymbol{l}_T+\boldsymbol{p}_{T2}-\boldsymbol{Q}_T)\right) \tag{24}$$

where $\phi_G^N\,(y,\boldsymbol{k}_T,-\boldsymbol{k}_T+\boldsymbol{Q}_T)$ denotes the probability to find a gluon with rapidity y and transverse momentum $k_\perp$, in the process with momentum transferred Q_T. In Eq. (24) $\bar{\alpha}_S = \alpha_S N_c/\pi$ with the number of colours equal to N_c. ϕ_G^N are the solutions of the BFKL evolution equation

$$\frac{\partial\phi_G^N\,(y,\boldsymbol{k}_T,-\boldsymbol{k}_T+\boldsymbol{Q}_T)}{\partial y} \;=\; \bar{\alpha}_S\int\frac{d^2k'_T}{2\pi}\,K\,(Q_T;k_T,k'_T)\;\phi_G^N\,(y,\boldsymbol{k'}_T,-\boldsymbol{k'}_T+\boldsymbol{Q}_T) \tag{25}$$
$$-\;\;\left(\omega_G\,(\boldsymbol{Q}_T-\boldsymbol{k}_T)\;+\;\omega_G\,(\boldsymbol{k}_T)\right)\phi_G^N\,(y,\boldsymbol{k}_T,-\boldsymbol{k}_T+\boldsymbol{Q}_T)$$

where

$$K\,(Q_T,k_T,k'_T) \;=\; \frac{1}{(\boldsymbol{k}_T-\boldsymbol{k'}_T)^2}\left\{\frac{k_T^2}{k_T'^2}\;+\;\frac{(\boldsymbol{Q}_T-\boldsymbol{k}_T)^2}{(\boldsymbol{Q}_T-\boldsymbol{k'}_T)^2}\;-\;\frac{(\boldsymbol{k}_T-\boldsymbol{k'}_T)^2}{k_T'^2\;(\boldsymbol{Q}_T-\boldsymbol{k'}_T)^2}\right\} \tag{26}$$
$$\omega_G\,(\boldsymbol{k}_T) \;=\; \frac{1}{2}\bar{\alpha}_S k_T^2\int\frac{d^2k'_T}{2\pi}\frac{1}{k_T'^2\;(\boldsymbol{k}_T-\boldsymbol{k'}_T)^2}$$

The typical momenta in ϕ_G^N is about $1/R_N$ or larger, (about $p_{T1}(p_{T2})$ or Q_s, where Q_s denotes the saturation scale. Bearing this in mind, and noting that $Q_T\sim 1/R_D \ll 1/R_N$ we can put $Q_T=0$, in the arguments of ϕ_G^N. This simplifies Eq. (24) reducing it to the following expression

$$\frac{d^2\sigma}{dy_1\,dy_2 d^2p_{T1}d^2p_{T2}}\,(Fig.\ 7) \;=\; \frac{d^2\sigma}{dy_1\;d^2p_{T1}}\,\frac{d^2\sigma}{dy_2\;d^2p_{T2}}\;\times\int d^2Q_T G_D^2\,(Q_T) \tag{27}$$

The diagram of Fig. 2-b in the LLA, simplifies the expression for the exchange of two BFKL Pomerons, but with more complicated vertices. Using Eq. (10) and considering $\bar{\alpha}_S\,(y_1-y_2)\leq 1$, we can write this exchange in the form that is represented in Fig. 8, and its contribution has the following form

$$\frac{d^2\sigma}{dy_1\,dy_2 d^2p_{T1}d^2p_{T2}}\,(Fig.\ 8) \;=\; \frac{1}{2}\left(\frac{2\pi\bar{\alpha}_S}{C_F}\right)^2\int d^2Q_T G_D\,(Q_T)\;G_D\left(\boldsymbol{Q}_T-\boldsymbol{p}_{T,12}\right) \tag{28}$$
$$\times\;\left(\int d^2k_T\;\phi_G^N\,(Y-y_1;\boldsymbol{k}_T,-\boldsymbol{k}_T+\boldsymbol{Q}_T)\;\Gamma_\mu\,(k_T,p_{T1})\;\Gamma_\mu\,(-\boldsymbol{k}_T+\boldsymbol{Q}_T,p_{T2})\;\phi_G^N\,(y_2;\boldsymbol{k}_T-\boldsymbol{p}_{T1},-\boldsymbol{k}_T+\boldsymbol{p}_{T2}+\boldsymbol{Q}_T)\right)$$
$$\times\;\left(\int d^2l_T\;\phi_G^N\,(Y-y_1;\boldsymbol{l}_T,-\boldsymbol{l}_T-\boldsymbol{Q}_T)\;\Gamma_\mu\,(l_T,p_{T1})\;\Gamma_\mu\,(-\boldsymbol{l}_T-\boldsymbol{Q}_T,p_{T2})\,\phi_G^N\,(y_2;\boldsymbol{l}_T-\boldsymbol{p}_{T2},-\boldsymbol{l}_T+\boldsymbol{p}_{T1}-\boldsymbol{Q}_T)\right)$$

Since $Q_T\sim 1/R_B \ll 1/R_N$ as well as $|\boldsymbol{Q}_T-\boldsymbol{p}_{T,12}|\sim 1/R_D \ll 1/R_N$, we can take both $Q_T=0$ and $p_{T,12}=0$, but it is not sufficient to reduce Eq. (28) to Eq. (12). In addition we need to assume that $\bar{\alpha}_S\,(y_1-y_2)\leq 1$. Making this assumption we can replace y_2 in $\phi_G^N\,(y_2;\boldsymbol{k}_T-\boldsymbol{p}_{T1},-\boldsymbol{k}_T+\boldsymbol{p}_{T2}+\boldsymbol{Q}_T)$ by y_1 and $Y-y_1$, in $\phi_G^N\,(Y-y_1;\boldsymbol{l}_T,-\boldsymbol{l}_T-\boldsymbol{Q}_T)$ by $Y-y_2$. After these changes Eq. (28) can be reduced to the following expression

$$\frac{d^2\sigma}{dy_1\,dy_2 d^2p_{T1}d^2p_{T2}}\,(Fig.\ 8) \;=\; \frac{d^2\sigma}{dy_1\;d^2p_{T1}}\,\frac{d^2\sigma}{dy_2\;d^2p_{T2}}\;\times\int d^2Q_T G_D\,(Q_T)\;G_D\left(\boldsymbol{Q}_T+\boldsymbol{p}_{T,12}\right) \tag{29}$$

Eq. (27) and Eq. (29) lead to the same correlation function ($C\,(R_D\,p_{T,12})$) Eq. (12) as in the Born approximation.

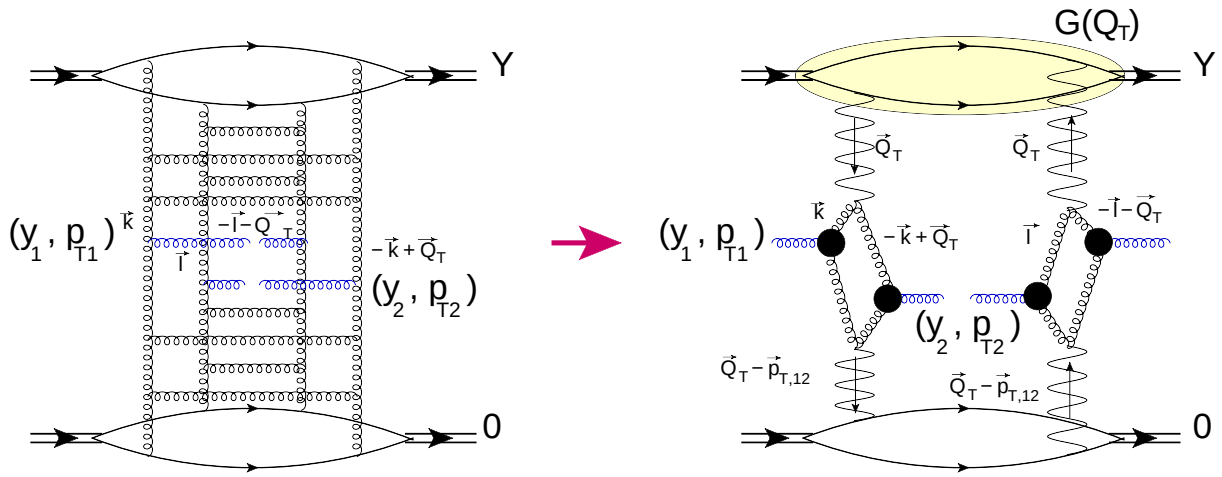

FIG. 8: The double inclusive production of two gluons with rapidities y_1 and y_2 and transverse momenta $\boldsymbol{p}_{T1}$ and $\boldsymbol{p}_{T2}$ for the exchange of two BFKL Pomerons which are denoted by wavy lines. This diagram is the LLA generalization of Fig. 2-b. The solid lines denote nucleons in the deuterons, which are represented by double lines.

B. $R_c \propto R_N$

In LLA the diagrams of the Born approximation of Fig. 3 can be generalized in the same way as has been discussed above. Fig. 3-a takes the form of Fig. 9 while the interference diagram of Fig. 3-b becomes Fig. 10.

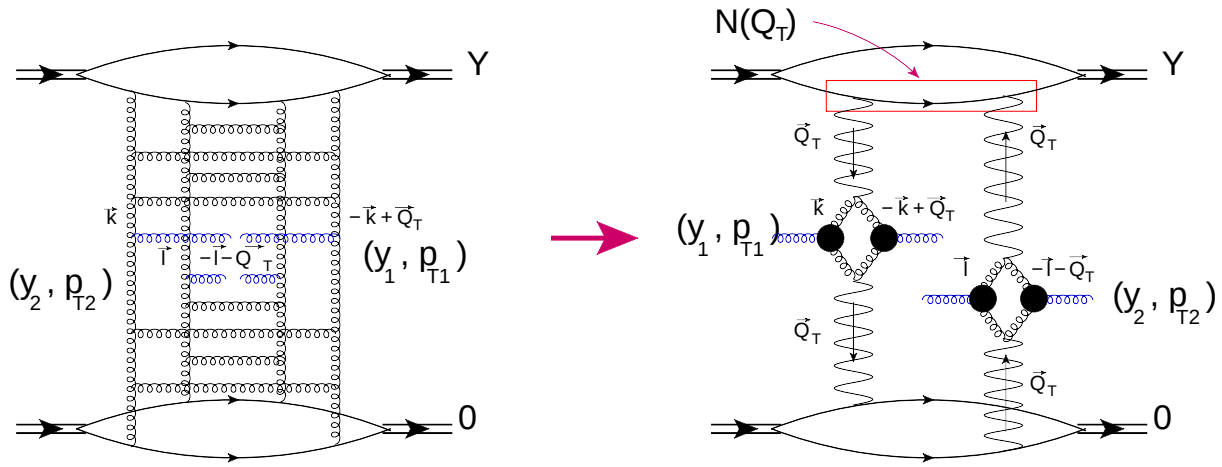

FIG. 9: The Mueller diagram[28] for the double inclusive production of two gluons with rapidities y_1 and y_2 and transverse momenta $\boldsymbol{p}_{T1}$ and $\boldsymbol{p}_{T2}$, for the exchange of two BFKL Pomerons which are denoted by wavy lines. This diagram is the LLA generalization of Fig. 3-a. The solid lines denote nucleons in the deuterons, which are illustrated by double lines.

The contribution of the diagram of Fig. 9 can be written as follows

$$\frac{d^2\sigma}{dy_1\,dy_2 d^2p_{T1} d^2p_{T2}}\,(Fig.\ 9) \;=\; \left(\frac{2\pi\bar{\alpha}_S}{C_F}\right)^2 \frac{1}{p^2_{T,1}\,p^2_{T2}} \int d^2Q_T\, N\left(Q_T\right)\, G^2_D\left(Q_T\right)$$
$$\times \left(\int d^2k_T\; \phi^N_G\left(Y-y_1;\boldsymbol{k}_T,-\boldsymbol{k}_T+\boldsymbol{Q}_T\right)\, \phi^N_G\left(y_1;\boldsymbol{k}_T-\boldsymbol{p}_{T1},-\boldsymbol{k}_T+\boldsymbol{p}_{T1}+\boldsymbol{Q}_T\right)\right)$$
$$\times \left(\int d^2l_T\; \phi^N_G\left(Y-y_2;\boldsymbol{l}_T,-\boldsymbol{l}_T-\boldsymbol{Q}_T\right)\, \phi^N_G\left(y_2;\boldsymbol{l}_T-\boldsymbol{p}_{T2},-\boldsymbol{l}_T+\boldsymbol{p}_{T2}-\boldsymbol{Q}_T\right)\right) \tag{30}$$

where $N\left(Q_T\right)$ denotes the integral over all energies of the imaginary part of the Pomeron-nucleon scattering amplitude.

This amplitude was introduced in Gribov's Pomeron calculus[26], but it has been proven that we can use this formalism in LLA of perturbative QCD[27]. $N\left(Q_T\right)$ has the following general form(see Fig. 11)

$$N\left(Q_T\right) \;=\; \underbrace{g^2\left(Q_T\right)}_{\text{elastic scattering}} \;+\; \underbrace{\sum_{M_i=m}^{M_0} g^2\left(Q_T;M_i\right)}_{\text{diffraction in low masses}} \;+\; \underbrace{\int_{M_0}\frac{dM^2}{M^2}\phi_G^N\left(y_M,Q_T=0;\{\dots\}\right)\,G_{3I\!P}\left(Q_T,\{\dots\}\right)}_{diffraction\,in\,high\,masses} \tag{31}$$

where $G_{3I\!P}$ is the triple BFKL Pomeron vertex, and $\{\dots\}$ denotes all transverse momenta which we need to integrate over. $y_M=\ln\left(M^2/M_0^2\right)$.

Fig. 11-b shows how all contributions correspond to the onium case, where we can use perturbative QCD for theoretical estimates.

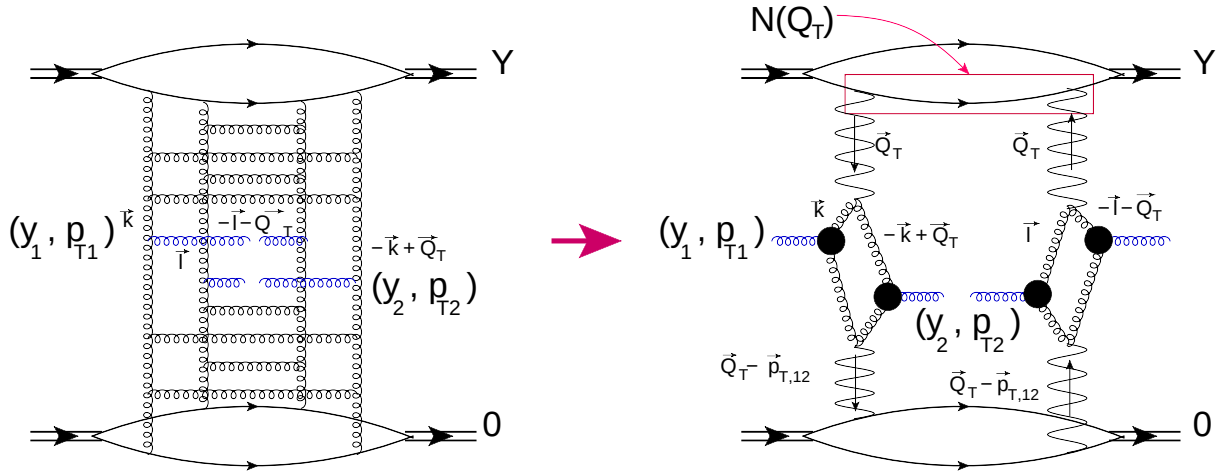

FIG. 10: The Mueller diagram for the double inclusive production of two gluons with rapidities y_1 and y_2 and transverse momenta $\boldsymbol{p}_{T1}$ and $\boldsymbol{p}_{T2}$, for the exchange of two BFKL Pomerons which are denoted by wavy lines. This diagram is the LLA generalization of Fig. 3-b. The solid lines denote nucleons in the deuterons, which are illustated by double lines.

Since $Q_T\sim 1/R_D\ll 1.R_N$, and all other transverse momenta in Fig. 9 are either of the order of $1/R_N$ or larger (of the order of p_{T1},p_{T2} or Q_s, where Q_s is the saturation scale), we can safely put $Q_T=0$ and reduce this contribution to the factorized form:

$$\frac{d^2\sigma}{dy_1\,dy_2 d^2p_{T1}d^2p_{T2}}\left(Fig.\ 9\right) \;=\; \frac{d^2\sigma}{dy_1\,d^2p_{T1}}\,\frac{d^2\sigma}{dy_2\,d^2p_{T2}}\,N\left(Q_T=0\right)\int d^2Q_T G_D\left(Q_T\right) \tag{32}$$

The contribution of the relevant diagram, which is shown in Fig. 10, can be written in the form:

$$\begin{aligned}
&\frac{d^2\sigma}{dy_1\,dy_2 d^2p_{T1}d^2p_{T2}}\left(Fig.\ 10\right) \;=\; \frac{1}{2}\left(\frac{2\pi\bar{\alpha}_S}{C_F}\right)^2\int d^2Q_T N\left(Q_T\right)\,G_D\left(\boldsymbol{Q}_T-\boldsymbol{p}_{T,12}\right)\\
\times\;&\left(\int d^2k_T\;\phi_G^N\left(Y-y_1;\boldsymbol{k}_T,-\boldsymbol{k}_T+\boldsymbol{Q}_T\right)\,\Gamma_\mu\left(k_T,p_{T1}\right)\,\Gamma_\mu\left(-\boldsymbol{k}_T+\boldsymbol{Q}_T,p_{T2}\right)\,\phi_G^N\left(y_2;\boldsymbol{k}_T-\boldsymbol{p}_{T1},-\boldsymbol{k}_T+\boldsymbol{p}_{T2}+\boldsymbol{Q}_T\right)\right)\\
\times\;&\left(\int d^2l_T\;\phi_G^N\left(Y-y_1;\boldsymbol{l}_T,-\boldsymbol{l}_T-\boldsymbol{Q}_T\right)\,\Gamma_\mu\left(l_T,p_{T1}\right)\,\Gamma_\mu\left(-\boldsymbol{l}_T-\boldsymbol{Q}_T,p_{T2}\right)\phi_G^N\left(y_2;\boldsymbol{l}_T-\boldsymbol{p}_{T2},-\boldsymbol{l}_T+\boldsymbol{p}_{T1}-\boldsymbol{Q}_T\right)\right)
\end{aligned} \tag{33}$$

Integration over Q_T leads to $\boldsymbol{Q}_T-\boldsymbol{p}_{T,12}\sim 1/R_D\ll 1/R_N$ and, therefore, as in the Born approximation we can put $\boldsymbol{Q}_T=\boldsymbol{p}_{T,12}$. In Eq. (33) we have two sources of $p_{T,12}$ behavior: $N\left(p_{T,12}\right)$ and ϕ_G^N. Replacing $\boldsymbol{Q}_T=\boldsymbol{p}_{T,12}$ we obtain

$$
\begin{aligned}
\frac{d^2\sigma}{dy_1\,dy_2 d^2p_{T1}d^2p_{T2}}\,(Fig.\ 10) \;&=\; \frac{1}{2}\left(\frac{2\pi\bar{\alpha}_S}{C_F}\right)^2\int d^2Q_T N\left(p_{T,12}\right)\,G_D\left(\boldsymbol{Q}_T-\boldsymbol{p}_{T,12}\right)\\
\times\;&\left(\int d^2k_T\;\phi_G^N\left(Y-y_1;\boldsymbol{k}_T,-\boldsymbol{k}_T+\boldsymbol{p}_{T,12}\right)\;\frac{1}{k_T^2\;\left(\boldsymbol{k}_T-\boldsymbol{p}_{T,12}\right)^2\left(\boldsymbol{k}_T-\boldsymbol{p}_{T,1}\right)^4}\phi_G^N\left(y_2;\boldsymbol{k}_T-\boldsymbol{p}_{T1},-\boldsymbol{k}_T+\boldsymbol{p}_{T1}\right)\right.\\
\times\;&\left.\left\{\frac{\left(\boldsymbol{k}_T-\boldsymbol{p}_{T,12}\right)^2\left(\boldsymbol{k}_T-\boldsymbol{p}_{T,1}\right)^2}{p_{T2}^2}+\frac{k_T^2\;\left(\boldsymbol{k}_T-\boldsymbol{p}_{T,1}-\boldsymbol{p}_{T,12}\right)^2}{p_{T2}^1}-p_{T,12}^2-p_{T,12}^2\frac{k_T^2\;\left(\boldsymbol{k}_T-\boldsymbol{p}_{T,12}\right)^2}{p_{T2}^1p_{T,2}^2}\right\}\right)\\
\times\;&\left(\int d^2l_T\;\phi_G^N\left(Y-y_1;\boldsymbol{l}_T,-\boldsymbol{l}_T-\boldsymbol{p}_{T,12}\right)\;\frac{1}{l_T^2\;\left(\boldsymbol{l}_T+\boldsymbol{p}_{T,12}\right)^2\left(\boldsymbol{l}_T-\boldsymbol{p}_{T,2}\right)^4}\phi_G^N\left(y_2;\boldsymbol{l}_T-\boldsymbol{p}_{T2},-\boldsymbol{l}_T+\boldsymbol{p}_{T2}\right)\right.\\
\times\;&\left.\left\{\frac{\left(\boldsymbol{l}_T+\boldsymbol{p}_{T,12}\right)^2\left(\boldsymbol{l}_T-\boldsymbol{p}_{T,1}\right)^2}{p_{T2}^2}+\frac{l_T^2\;\left(\boldsymbol{l}_T-\boldsymbol{p}_{T,2}\right)^2}{p_{T2}^1}-p_{T,12}^2-p_{T,12}^2\frac{l_T^2\;\left(\boldsymbol{l}_T+\boldsymbol{p}_{T,12}\right)^2}{p_{T2}^1p_{T,2}^2}\right\}\right)
\end{aligned}
\tag{34}
$$

The products of $G_\mu G_\mu$ are written in Eq. (34) $\{\dots\}$ explicitly using Eq. (6), and ϕ_D^N are the solution of Eq. (25). Recall that $\phi_D^N\left(\boldsymbol{k}_T,-\boldsymbol{k}_T+\boldsymbol{Q}_T\right)$ vanishes both at $k_T\to 0$ and $\boldsymbol{k}_T-\boldsymbol{Q}_T\to 0$. Since the products of G_μ vanish at $\boldsymbol{k}_T-\boldsymbol{p}_{T1}\to 0$ or $\boldsymbol{l}_T-\boldsymbol{p}_{T2}\to 0$, respectively, we can conclude that the integrals over k_T and l_T do not have large contributions at k_T of the order of p_{T1}, and at l_T of the order of p_{T2}.

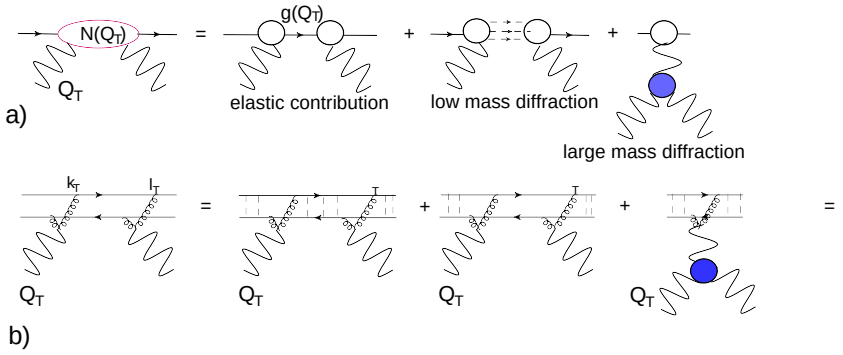

FIG. 11: The structure of the amplitude $N\left(Q_T\right)$: Fig. 11-a for the BFKL Pomeron-nucleon interaction and Fig. 11-b for the BFKL Pomeron-onium interactions. The blob shows the triple BFKL Pomeron vertex which is the same for both figures. The dashed vertical lines describe the Coulomb gluons that create the bound state: onium.

In the appendix we show that the typical value of Q_T for the BFKL Pomeron $\phi_G^N\left(Y;k_T',k_T,Q_T\right)$ is determined by the smallest value of transverse momentum $Q_T\sim min\{k_{;T}\,,k_T\}$. In our case this means that $Q_T=p_{T,12}\sim 1/R_N\gg p_{T1}$ and/or p_{T2}.

Therefore, we can re-write Eq. (34) as follows:

$$
\begin{aligned}
\frac{d^2\sigma}{dy_1\,dy_2 d^2p_{T1}d^2p_{T2}}\,(Fig.\ 10) \;&=\; \frac{1}{2}\left(\frac{2\pi\bar{\alpha}_S}{C_F}\right)^2\frac{1}{p_{T1}^2\,p_{T2}^2}\int d^2Q_T N\left(p_{T,12}\right)\,G_D\left(\boldsymbol{Q}_T-\boldsymbol{p}_{T,12}\right)\\
&\times\;\left(\int d^2k_T\;\phi_G^N\left(Y-y_1;\boldsymbol{k}_T,-\boldsymbol{k}_T\right)\;\phi_G^N\left(y_2;\boldsymbol{k}_T-\boldsymbol{p}_{T1},-\boldsymbol{k}_T+\boldsymbol{p}_{T1}\right)\right)\\
&\times\;\left(\int d^2l_T\;\phi_G^N\left(Y-y_1;\boldsymbol{l}_T,-\boldsymbol{l}_T\right)\;\phi_G^N\left(y_2;\boldsymbol{l}_T-\boldsymbol{p}_{T2},-\boldsymbol{l}_T+\boldsymbol{p}_{T2}\right)\right)
\end{aligned}
\tag{35}
$$

In Eq. (35) we introduce $\phi_G^N\left(\boldsymbol{k}_t,-\boldsymbol{k}_T\right)=(1/k_T^2)\phi_G^N\left(\boldsymbol{k}_t,-\boldsymbol{k}_T\right)(Eq.\ (34))$. Comparing Eq. (32) and Eq. (35), one can see that the correlation function is equal to

$$
C\left(R_N^2\,p_{T,12}^2\right)\;=\;N\left(p_{12}^2\right) \tag{36}
$$

for $\bar{\alpha}_S(y_1-y_2)\leq 1$.

The three terms of $N(Q_T)$ are shown in Fig. 11-a. The first contribution $N(Q_T) = g^2(Q_T)$, can easily be evaluated from the differential elastic cross section, which is proportional to $g^4(Q_T)$. Recall, that the BFKL Pomeron does not generate the shrinkage of the diffraction peak seen in the experimental data. This indicates that the exchange of the single BFKL Pomeron is not sufficient to describe the high energy amplitude, and we need to use a more phenomenological approach to describe the elastic contribution to the correlation function (see Ref.[4] in which we tried to describe these correlations using a particular model for high energy scattering, which is based on CGC/saturation approach).

For the onium, $g(Q_T)$ can be calculated (see Fig. 11-b and Eq. (B5)) in the following way

$$\begin{aligned} g(Q_T) = V^{\rm onium}(\boldsymbol{Q}_T) &= \int d^2k'_T I_P(\boldsymbol{k}_T, -\boldsymbol{k'}_T + \boldsymbol{Q}_T) V^{\rm pr}(\boldsymbol{k'}_T, \boldsymbol{Q}_T) \\ &= \int d^2k'_T \left(F(Q_T) - F(2\boldsymbol{k'}_T - \boldsymbol{Q}_T)\right) V^{\rm pr}_{\frac{1}{2}}\left(\boldsymbol{k'_T}, \boldsymbol{Q}_T\right) \end{aligned} \tag{37}$$

where $V^{\rm pr}$ is determined by Eq. (B4). In Eq. (37) $k'_T \sim 1/R_N \ll k_T$. Assuming that $F(Q_T)$ of Eq. (14) is equal to $1/\left(1 + R_N^2 Q_T^2\right)$, we find that at large Q_T, $g(R_N Q_T)$ decreases as $1/Q_T$.

The second term of Fig. 11-b can be evaluated from the process of diffraction dissociation in the region of small masses. However, we need to use a model for this term to be able to extract its Q_T dependence from the experimental data. For example, we can replace the sum of possible produced diffractive states by one state, as has been done in Ref.[4]. For the onium state this term has the following form

$$N_{\rm diff}(Q_T) = \int d^2k'_T \int d^2l'_T I_P(\boldsymbol{k}_T, \boldsymbol{l}_T, -\boldsymbol{l}_T + \boldsymbol{Q}_T, -\boldsymbol{k}_T + \boldsymbol{Q}_T)\ V^{\rm pr}(\boldsymbol{k'}_T; \boldsymbol{Q}_T)\ V^{\rm pr}(\boldsymbol{l'}_T; \boldsymbol{Q}_T) \tag{38}$$

where I_P is taken from Eq. (15).

Using Eq. (B4) we calculate $N_{\rm diff}(Q_T)$ which decreases as $1/Q_T^2$ at large Q_T.

C. $R_c \propto 1/Q_s$

The last term in Fig. 11-a, gives the contribution of large mass production in the diffraction dissociation process. The Q_T dependence of this term, is determined by the triple BFKL Pomeron vertex in perturbative QCD (see Fig. 12). Therefore, this term generates correlations, whose length is determined by the BFKL Pomeron structure, and it is closely related to the typical saturation momentum Q_s.

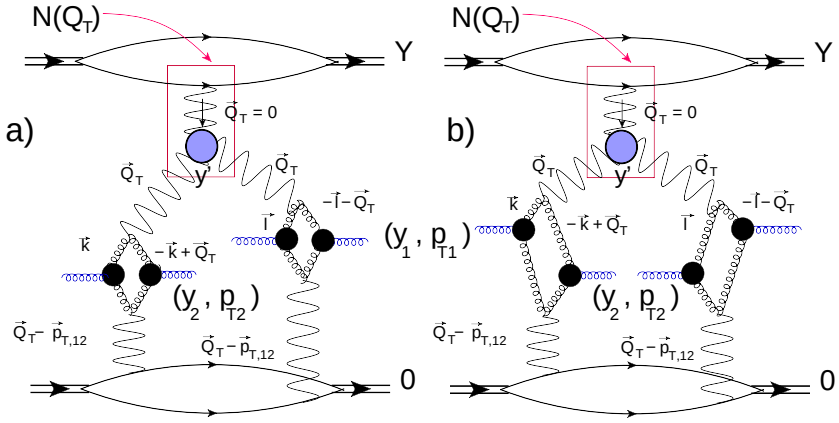

FIG. 12: The large mass diffraction contribution to $N(Q_T)$: the source for the correlation length of about $1/Q_s$. The blue blob denotes the triple BFKL Pomeron vertex. The red square indicates the contribution of $N(Q_T)$, which includes the integration over rapidity y'.

Comparing Fig. 12 with Fig. 9 and Fig. 10, one can see that the difference is only in expression for $N(Q_T)$ which has the following form

$$N_{\rm large\,mass\,diffraction}(Q_T) = \int d\,y'\,\phi_G^N(Y - y'; Q_T = 0; q_T, q'_T)\, d^2q'_T G_{3I\!P}(q'_T; k'_T, l'_T, Q_T) \tag{39}$$

We can obtain the form of $G_{3I\!P}$ in momentum space starting from the coordinate representation, where the contribution of the triple Pomeron diagram of Fig. 13 is known[29, 30]:

$$\bar{\alpha}_S \int \frac{d^2x_0\, d^2x_1\, d^2x_2}{x_{01}^2\, x_{02}^2\, x_{21}^2} N\left(x'_{01}, x_{01}; \boldsymbol{b}-\boldsymbol{b'}; Y-y'\right)\, N\left(x'_{02}, x_{02}; \boldsymbol{b'}-\frac{1}{2}\boldsymbol{x}_{21}; y'-y_1\right)\, N\left(x'_{21}, x_{21}; \boldsymbol{b'}-\frac{1}{2}\boldsymbol{x}_{02}; y'-y_2\right) \tag{40}$$

Introducing[18]

$$N\left(x_{01}, b; Y\right) \;=\; x_{01}^2 \int d^2k d^2Q_T\, e^{i\boldsymbol{k}_T\cdot\boldsymbol{x}_{01}\,+\,i\,\boldsymbol{Q}_T\cdot\boldsymbol{b}} N\left(k_T, Q_T\right) \tag{41}$$

we see that Eq. (40) can be re-written in the form

$$\bar{\alpha}_S \int d^2q'_T\, N\left(q_T, q'_T, Q_T=0, Y-y'\right)\, G_{3I\!P}\left(q'_T; k'_T, l'_T, Q_T\right) N\left(k'_T, k_T, Q_T, y'-y_1\right)\, N\left(l'_T, l_T, -Q_T, y'-y_2\right) \tag{42}$$

with

$$G_{3I\!P}\left(q'_T; k'_T, l'_T, Q_T\right) \;=\; \delta^{(2)}\left(\boldsymbol{k'}_T\,-\boldsymbol{q'}\,+\frac{1}{2}\boldsymbol{Q}_T\right)\,\delta^{(2)}\left(\boldsymbol{l'}_T\,-\boldsymbol{q'}\,-\frac{1}{2}\boldsymbol{Q}_T\right) \tag{43}$$

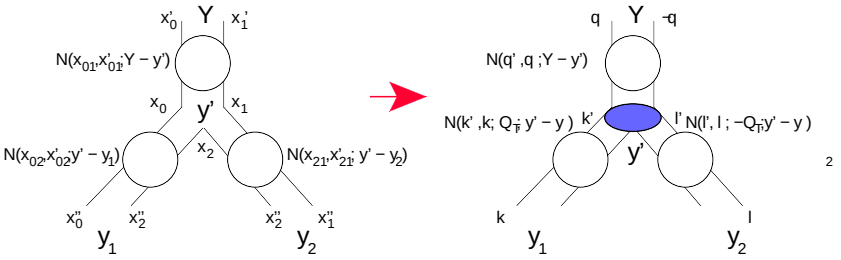

FIG. 13: The triple BFKL Pomeron vertex in coordinate and momentum representations. The blue blob denotes the triple Pomeron vertex

In Eq. (39) we use the following notation for $\phi_G^N\left(Y-y'; Q_T=0; k_i, k_f\right)$: $Y-y'$ is the rapidity, Q_T is the momentum transfer of the BFKL Pomeron, k_i and k_f are initial and final transverse momenta. Plugging Eq. (43) in the general expression for the interference diagram of Fig. 12-b, we see that instead of Eq. (34) we obtain

$$\begin{aligned}
&\frac{d^2\sigma}{dy_1\, dy_2 d^2p_{T1} d^2p_{T2}}\left(Fig.\ 12-b\right) \;= \\
&\frac{1}{2}\left(\frac{2\pi\bar{\alpha}_S}{C_F}\right)^2 \int d^2Q_T G_D\left(\boldsymbol{Q}_T-\boldsymbol{p}_{T,12}\right)\, \int d\,y' \int \phi_G^N\left(Y-y'; Q_T=0; q_T, q'_T\right)\, d^2q'_T \\
\times\; &\left(G^{\rm BFKL}\left(y'-y_1; p_{T,12}; \boldsymbol{q'}_T-\frac{1}{2}\boldsymbol{p}_{T,12}, k_T\right)\, \frac{1}{k_T^2\,\left(\boldsymbol{k}_T-\boldsymbol{p}_{T,12}\right)^2\left(\boldsymbol{k}_T-\boldsymbol{p}_{T,1}\right)^4} G^{\rm BFKL}\left(y_2; 0; \boldsymbol{k}_T-\boldsymbol{p}_{T1}, k_N\right)\right. \\
\times\; &\left.\left\{\frac{\left(\boldsymbol{k}_T-\boldsymbol{p}_{T,12}\right)^2\left(\boldsymbol{k}_T-\boldsymbol{p}_{T,1}\right)^2}{p_{T2}^2} + \frac{k_T^2\,\left(\boldsymbol{k}_T-\boldsymbol{p}_{T,1}-\boldsymbol{p}_{T,12}\right)^2}{p_{T2}^1} - p_{T,12}^2 - p_{T,12}^2\frac{k_T^2\,\left(\boldsymbol{k}_T-\boldsymbol{p}_{T,12}\right)^2}{p_{T2}^1 p_{T,2}^2}\right\}\right) \\
\times\; &\left(\int d^2l_T\, G^{\rm BFKL}\left(y'-y_1; p_{T,12}, \boldsymbol{q'}_T+\frac{1}{2}\boldsymbol{p}_{T,12}, l_T\right)\, \frac{1}{l_T^2\,\left(\boldsymbol{l}_T+\boldsymbol{p}_{T,12}\right)^2\left(\boldsymbol{l}_T-\boldsymbol{p}_{T,2}\right)^4} G^{\rm BFKL}\left(y_2; 0; \boldsymbol{l}_T-\boldsymbol{p}_{T2}, l_N\right)\right. \\
\times\; &\left.\left\{\frac{\left(\boldsymbol{l}_T+\boldsymbol{p}_{T,12}\right)^2\left(\boldsymbol{l}_T-\boldsymbol{p}_{T,1}\right)^2}{p_{T2}^2} + \frac{l_T^2\,\left(\boldsymbol{l}_T-\boldsymbol{p}_{T,2}\right)^2}{p_{T2}^1} - p_{T,12}^2 - p_{T,12}^2\frac{l_T^2\,\left(\boldsymbol{l}_T+\boldsymbol{p}_{T,12}\right)^2}{p_{T2}^1 p_{T,2}^2}\right\}\right)
\end{aligned} \tag{44}$$

The main difference between Eq. (44) and Eq. (34), is that q'_T is larger than $q_T \approx 1/R_N$. Indeed, the typical value of $q'_T = Q_s\left(Y-y'\right) \sim \left(1/R_N^2\right)\exp\left(\lambda\left(Y-y'\right)\right)$, where $\lambda = \omega\left(\gamma_{cr}, 0\right)/\left(1-\gamma_{cr}\right.$ with $\gamma_{cr} = 0.37$ in leading order of perturbative QCD [18],

From Eq. (A16) one can see that each $\phi_D^N(Y-y') \propto e^{\omega\left(\frac{1}{2},0\right)\left(Y-y'\right)}$, $\phi_D^N(y'-y_1) \propto e^{\omega\left(\frac{1}{2},0\right)\left(y'-y_1\right)}$, and $\phi_D^N(y'-y_2) \propto e^{\omega\left(\frac{1}{2},0\right)\left(y'-y_2\right)}$, since $\gamma = \frac{1}{2} + i\nu$ with small ν. Therefore, integration over y' results in $Y - y' \sim 1/\omega\left(\frac{1}{2},0\right) \propto 1/\bar{\alpha}_S$ while $y'-y_1$ and $y'-y_2$ are large (of the order of Y). Since $Y-y' \ll y'-y_1 (Y-y' \ll y'-y_2)$ we can use the factorized formula of Eq. (A15) for $\phi_G^N\left(y'-y_1; p_{T,12}; \boldsymbol{q'}_T - \frac{1}{2}\boldsymbol{p}_{T,12}, k_T\right)$ and for $\phi_G^N\left(y'-y_1; p_{T,12}, \boldsymbol{q'}_T + \frac{1}{2}\boldsymbol{p}_{T,12}, l_T\right)$. Using Eq. (A15) we find that $p_{T,12}$ will be determined by the lowest momenta in the BFKL Pomeron with $y'-y_1$, and it will have the form

$$C\left(p_{T,12}\right) \;\propto\; \int d^2q'_T I_{-\gamma}\left(q'_T\right) V_\gamma\left(\boldsymbol{q'}_T - \frac{1}{2}\boldsymbol{Q}_T, \boldsymbol{Q}_T\right) V_\gamma\left(\boldsymbol{q'}_T + \frac{1}{2}\boldsymbol{Q}_T, \boldsymbol{Q}_T\right) \tag{45}$$

where V is determined by Eq. (A12), and $Q_T = p_{T,12}$. In Eq. (45) we can put $\gamma = \frac{1}{2}$, assuming $y'-y_1$ is suffiently large, that we can neglect ν.

IV. BOSE-EINSTEIN CORRELATION FUNCTION IN THE NUCLEON-NUCLEON INTERACTION

In this section we discuss the Bose-Einstein correlations in nucleon-nucleon scattering. The Mueller diagrams for the square of the diagrams Fig. 1-a and Fig. 1-b, and for the interference diagrams, are shown in Fig. 14. This differs from the diagrams that have been discussed above, only in the appearance of the second $N\left(Q_T\right)$, which reflects the fact that we do not have small (about $1/R_D$) momenta in this process. Note, we can use perturbative QCD only if $p_{T1} \sim p_{T2} \gg 1/R_N$. Recalling that the Q_T dependence of the BFKL Pomeron is determined by the smallest transverse momentum, we conclude that in Fig. 14 the Q_T dependence is determined by the function $N\left(Q_T\right)$. For the first two contributions to $N\left(Q_T\right)$ (see Fig. 11-a), this is accurate to the order of $1/\left(R_N\, p_{T1}\right)$. For the third contribution of the large mass diffraction, the accuracy is about Q_s/p_{T1}, where Q_s denotes the saturation momentum of the BFKL Pomeron with rapidity $Y-y'$.

In spite of the fact that we indicate in Fig. 11-a the sources of experimental information on each contribution, the situation turns out to be more complicated. As an example, we discuss the elastic contribution. This gives $N\left(Q_T\right) = g^2\left(Q_T\right)$, where $g\left(Q_T\right)$ is the Pomeron-hadron vertex. At first sight we can extract this vertex directly from the experimental values of $d\sigma_{el}/dt$. However, this is certainly not correct. Indeed, the BFKL Pomeron cannot explain the shrinkage of the diffraction peak which is seen experimentally, and which gives almost a half of the slope of the elastic cross section for the energy range $W = 40 - 7000\, GeV$[32]. In the only model[33] for the soft interaction at high energy that is based on the BFKL Pomeron and Colour Glass Condensate (CGC) approach[34, 35], the effective shrinkage of the diffraction peak stems from strong shadowing corrections, which lead to an elastic amplitude that is different from that for the exchange of the BFKL Pomeron. However, it turns out that the most essential shadowing corrections originate from the BFKL Pomeron interaction of two scattering hadrons. Such corrections do not contribute to the inclusive cross sections, as well as to the correlation due to AGK cutting rules[20].

It turns out to be an even more complicated problem to extract from the experimental data, the diffraction contribution to $N\left(Q_T\right)$ in the region of small masses. The lack of a theory, as well as insufficient experimental data, especially of the momentum transfer distribution of the diffractively produced state with fixed mass, lead to the necessity of modeling this process. The two extreme cases of such a modeling illustrates the difficulties: in our model [33] the rich variety of the produced states were replaced by a single state: and in the constituent quark model[36] the small mass diffraction stems from production of the state of free three constituent quarks. In our model the typical slope for $g_{diff}\left(Q_T\right) \propto \exp\left(-B\, Q_T^2\right)$ turns out to be $1/4$ from the elastic slope, while in the CQM the size of the constituent quark is very small.

Taking the above into consideration, the uncertainties in the large mass diffraction term look small, and for the triple BFKL Pomeron vertex, both the value and transverse momenta dependence follow directly from the Balitsky-Kovchegov equation[34]. Bearing this in mind, we can write the expression for the interference diagram of Fig. 14, for the large mass diffraction contribution (see Fig. 11). As we have discussed in this case $Q_T \sim Q_s\left(Y-y'\right) \;\ll\; \min\left\{p_{T1}(p_{T2}), Q_s\left(y'-y_1\right)\right\}$, $|\boldsymbol{Q}_T - \boldsymbol{p}_{T,12}| \sim\; Q_s\left(Y-y'\right) \;\ll\; \min\left\{p_{T1}(p_{T2}), Q_s\left(y'-y_1\right)\right\}$, and $k'_T \sim \min\left\{p_{T1}(p_{T2}), Q_s\left(y'-y_1\right)\right\}$ ($l'_T \sim \min\left\{p_{T1}(p_{T2}), Q_s\left(y'-y_1\right)\right\}$). Hence, we can use the factorized form for ϕ_N^G given by Eq. (A15) and Eq. (A16).

Finally, the large mass contribution for the interference diagram takes the form

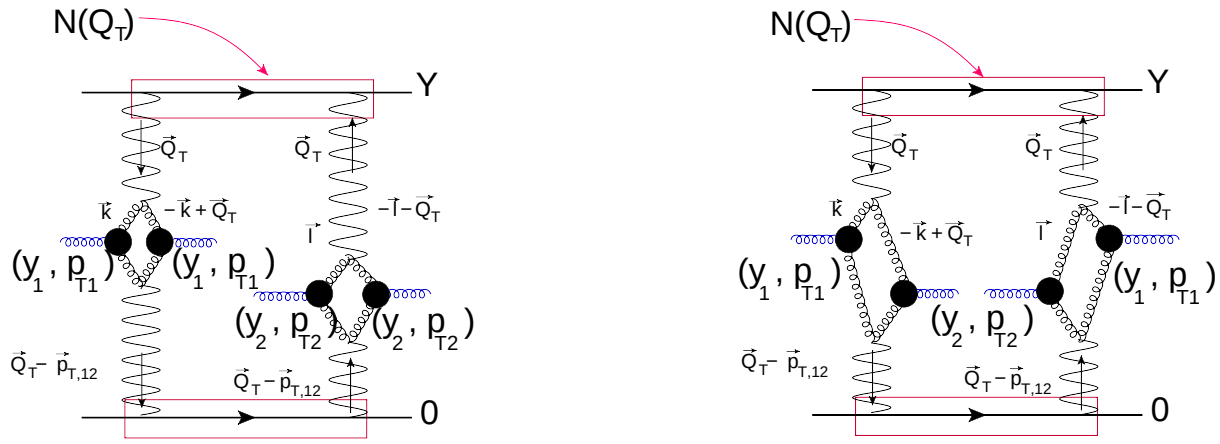

FIG. 14: The Mueller diagram for the double inclusive production of two gluons with rapidities y_1 and y_2 and transverse momenta $\boldsymbol{p}_{T1}$ and $\boldsymbol{p}_{T2}$ in the nucleon-nucleon interaction. The BFKL Pomerons are denoted by wavy lines. The first diagram corresponds to the square of the amplitude for two parton showers production, while the second diagram describes the interference.

$$
\begin{aligned}
&\frac{d^2\sigma}{dy_1\,dy_2 d^2p_{T1} d^2p_{T2}}\,(Fig.\ 14, \text{interference diagram}) \;=\\
&\frac{1}{2}\frac{1}{N_c^2-1}\left(\frac{2\pi\bar{\alpha}_S}{C_F}\right)^2\frac{1}{p_{T1}^2\,p_{T2}^2}\int d\,y'\int\phi_G^N\left(Y-y';Q_T=0;q_N,q_T'\right)\\
&\int d^2q_T'\,d^2k_T G^{\rm BFKL}\left(y'-y_1;Q_T;\boldsymbol{q'}_T-\frac{1}{2}\boldsymbol{Q}_T,k_T\right)\int dy''\,G^{\rm BFKL}\left(y_2-y'';\boldsymbol{Q}_T-\boldsymbol{p}_{T,12};\boldsymbol{k}_T-\boldsymbol{p}_{T1},\boldsymbol{m}_T'-\frac{1}{2}\left(\boldsymbol{Q}_T-\boldsymbol{p}_{T,12}\right)\right)\\
&\times\int d^2l_T\,d^2m_T'\,G^{\rm BFKL}\left(y'-y_1;Q_T,\boldsymbol{q'}_T+\frac{1}{2}\boldsymbol{Q}_T,l_T\right)\;G^{\rm BFKL}\left(y_2-y'';\boldsymbol{Q}_T-\boldsymbol{p}_{T,12};\boldsymbol{l}_T-\boldsymbol{p}_{T2},\boldsymbol{m}_T'+\frac{1}{2}\left(\boldsymbol{Q}_T-\boldsymbol{p}_{T,12}\right)\right)\\
&\times\phi_G^N\left(y'';Q_T=0;m_N,m_T'\right)
\end{aligned}
\tag{46}
$$

In the diagram for the square of the amplitude we can put $\boldsymbol{p}_{T,12}=0$. Thus, the correlation function with the correlation length of the order of $1/Q_s\,(Y-y')$, takes the following form

$$
C\left(p_{T,12}/Q_s\right) \;=\; \frac{1}{2}\frac{1}{N_c^2-1}\,\frac{N}{D} \tag{47}
$$

where

$$
\begin{aligned}
N \;=\;&\int d^2Q_T\int d\,y'\int\phi_G^N\left(Y-y';Q_T=0;q_N,q_T'\right)\\
&\int d^2q_T'\,d^2k_T G^{\rm BFKL}\left(y'-y_1;Q_T;\boldsymbol{q'}_T-\frac{1}{2}\boldsymbol{Q}_T,k_T\right)\int dy''\,G^{\rm BFKL}\left(y_2-y'';\boldsymbol{Q}_T-\boldsymbol{p}_{T,12};\boldsymbol{k}_T-\boldsymbol{p}_{T1},\boldsymbol{m}_T'-\frac{1}{2}\left(\boldsymbol{Q}_T-\boldsymbol{p}_{T,12}\right)\right)\\
\times&\int d^2l_T\,d^2m_T'\,G^{\rm BFKL}\left(y'-y_1;Q_T,\boldsymbol{q'}_T+\frac{1}{2}\boldsymbol{Q}_T,l_T\right)\;G^{\rm BFKL}\left(y_2-y'';\boldsymbol{Q}_T-\boldsymbol{p}_{T,12};\boldsymbol{l}_T-\boldsymbol{p}_{T2},\boldsymbol{m}_T'+\frac{1}{2}\left(\boldsymbol{Q}_T-\boldsymbol{p}_{T,12}\right)\right)\\
\times&\;\phi_G^N\left(y'';Q_T=0;m_N,m_T'\right)
\end{aligned}
\tag{48}
$$

and

$$
\begin{aligned}
D \;=\;&\int d^2Q_T\int d\,y'\int\phi_G^N\left(Y-y';Q_T=0;q_N,q_T'\right)\\
&\int d^2q_T'\,d^2k_T\phi_G^N\left(y'-y_1;Q_T;\boldsymbol{q'}_T-\frac{1}{2}\boldsymbol{Q}_T,k_T\right)\int dy''\,\phi_G^N\left(y_2-y'';\boldsymbol{Q}_T-\boldsymbol{p}_{T,12};\boldsymbol{k}_T-\boldsymbol{p}_{T1},\boldsymbol{m}_T'-\frac{1}{2}\boldsymbol{Q}_T\right)\\
\times&\int d^2l_T\,d^2m_T'\,\phi_G^N\left(y'-y_1;Q_T,\boldsymbol{q'}_T+\frac{1}{2}\boldsymbol{Q}_T,l_T\right)\;\phi_G^N\left(y_2-y'';\boldsymbol{Q}_T;\boldsymbol{l}_T,\boldsymbol{m}_T'+\frac{1}{2}\boldsymbol{Q}_T\right)\\
\times&\;\phi_G^N\left(y'';Q_T=0;m_N,m_T'\right)
\end{aligned}
\tag{49}
$$

The rather long algebraic expression of Eq. (48) and Eq. (49) can be simplified using Eq. (A17) and they take the following forms

$$
\begin{aligned}
N &= \int d^2Q_T \int dy' e^{2\omega\left(\frac{1}{2},0\right)y'} d^2q'_T \phi_G^N\left(Y-y';Q_T=0;q_N,q'_T\right) \frac{V_{\frac{1}{2}}\left(\boldsymbol{q'_T},\boldsymbol{Q}_T-\frac{1}{2}\boldsymbol{p}_{T,12}\right) V_{\frac{1}{2}}\left(\boldsymbol{q'_T},\boldsymbol{Q}_T+\frac{1}{2}\boldsymbol{p}_{T,12}\right)}{\left|\boldsymbol{Q}_T-\frac{1}{2}\boldsymbol{p}_{T,12}\right|\left|\boldsymbol{Q}_T+\frac{1}{2}\boldsymbol{p}_{T,12}\right|} \\
&\times \int dy'' e^{2\omega\left(\frac{1}{2},0\right)y''} d^2l'_T \phi_G^N\left(y'';Q_T=0;l_N,l'_T\right) \frac{V_{\frac{1}{2}}\left(\boldsymbol{l'_T},\boldsymbol{Q}_T\right) V_{\frac{1}{2}}\left(\boldsymbol{l'_T},\boldsymbol{Q}_T\right)}{Q_T^2} \qquad (50) \\
D &= \int d^2Q_T \int dy' e^{2\omega\left(\frac{1}{2},0\right)y'} d^2q'_T \phi_G^N\left(Y-y';Q_T=0;q_N,q'_T\right) \frac{V_{\frac{1}{2}}\left(\boldsymbol{q'_T},\boldsymbol{Q}_T\right) V_{\frac{1}{2}}\left(\boldsymbol{q'_T},\boldsymbol{Q}_T\right)}{Q_T^2} \\
&\times \int dy'' e^{2\omega\left(\frac{1}{2},0\right)y''} d^2l'_T \phi_G^N\left(y'';Q_T=0;l_N,l'_T\right) \frac{V_{\frac{1}{2}}\left(\boldsymbol{l'_T},\boldsymbol{Q}_T\right) V_{\frac{1}{2}}\left(\boldsymbol{l'_T},\boldsymbol{Q}_T\right)}{Q_T^2} \qquad (51)
\end{aligned}
$$

V. $\bar{\alpha}_S\left(y_1-y_2\right) \gg 1$

All our previous estimates were performed for small rapidity difference: $\bar{\alpha}_S|y_1-y_2| \leq 1$. In this section we discuss large rapidity differences ($\bar{\alpha}_S|y_1-y_2| \geq 1$). For simplicity, we consider only correlations with the typical length of the order of R_D. In other words, we discuss the generalization of Fig. 7 and Fig. 8 to the case of large $y_{12}=|y_1-y_2|$. This generalization is shown in Fig. 15 for the interference diagrams. The new features here are that at rapidity $y'_1<y_1$, we need to emit an additional gluon, and integrate over both its rapidity (y'_1) and its transferred momentum (p'_{T1}). Indeed, without this emission the ladder between rapidities y'_1 and y'_2 in Fig. 15-b will be in the octet state of color SU_3. The main idea is, that the principle contribution stems from $p'_{T1} \ll p_{T1}$. In this case the BFKL Pomeron between rapidities y'_1 and y'_2 has the momentum transfer which is equal to p_{T1}. After emission of two extra gluons with rapidities y'_2 and y_2, we obtain that the lower BFKL Pomeron, that has momentum transfer $p_{T,12}$, as in Fig. 8-b. In this diagram $Q_T \propto 1/R_D$, and can be put equal to zero in all parts of the diagrams, except of $G\left(Q_T\right)$ and $G\left(\boldsymbol{Q}_T-\boldsymbol{p}_{T,12}\right)$.

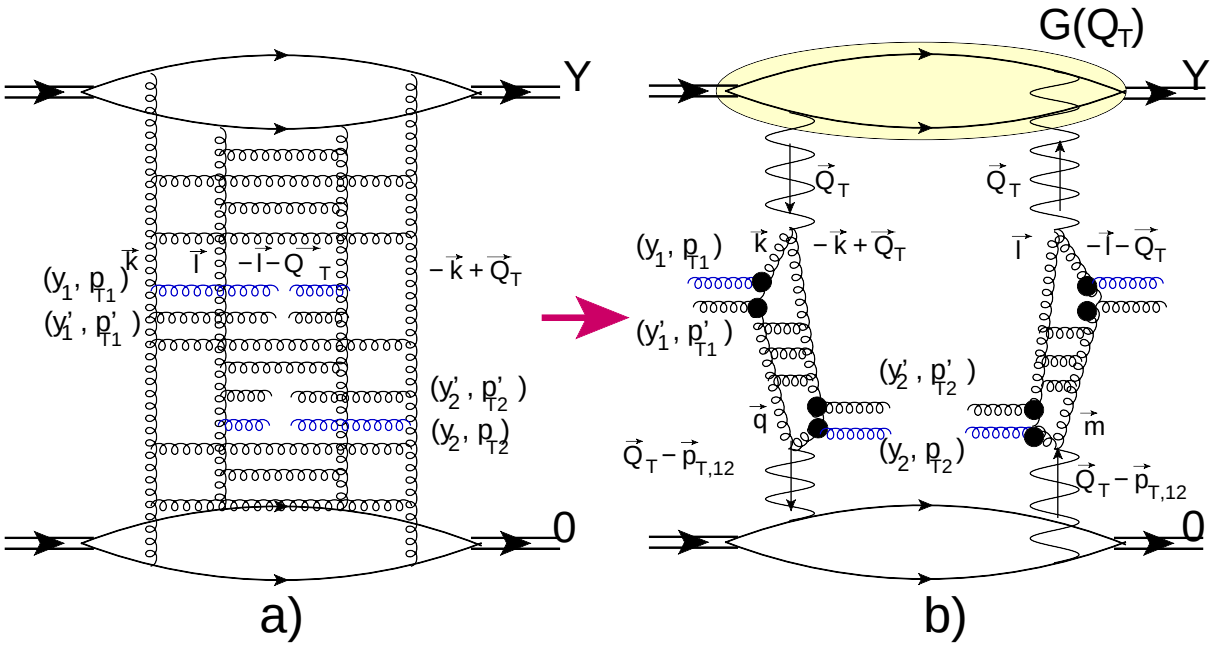

FIG. 15: The double inclusive production of two gluons with rapidities y_1 and y_2 in the case of large $|y_1-y_2|$ ($\bar{\alpha}_S\,|y_1-y_2| \gg 1$) and transverse momenta $\boldsymbol{p}_{T1}$ and $\boldsymbol{p}_{T2}$, for the exchange of two BFKL Pomerons which are denoted by wavy lines. This diagram is the LLA generalization of Fig. 8. The solid lines denote nucleons in the deuterons, which are illustrated by double lines. Note, that the ladder, shown in Fig. 15-b, represents the BFKL Pomeron with the momentum transferred $\boldsymbol{p}_{T1}+\boldsymbol{p}'_{T1} \approx \boldsymbol{p}_{T1}$ for $p'_{T1} \ll p_{T2}$ (see the text).

First, we need to integrate over p'_{T1}. The vertex of the emission is shown in Fig. 16 which can be written as

$$\bar{\alpha}_S^2\,\Gamma_\mu\left(\boldsymbol{k}_T,\boldsymbol{p}_{T1}\right)\,\Gamma_\mu\left(\boldsymbol{l}_T,\boldsymbol{p}_{T1}\right)\,\frac{1}{k_T'^2\,l_T'^2}\Gamma_\nu\left(\boldsymbol{k}'_T,\boldsymbol{p}_{T1}\right)\,\Gamma_\nu\left(\boldsymbol{l}'_T,\boldsymbol{p}_{T1}\right)\,\frac{1}{k_T''^2\,l_T''^2} \tag{52}$$

with $\boldsymbol{k}'_T=\boldsymbol{k}_T-\boldsymbol{p}_{T1}$ and $\boldsymbol{k}''_T=\boldsymbol{k}'_T-\boldsymbol{p}'_{T1}=\boldsymbol{k}_T-\boldsymbol{p}_{T1}-\boldsymbol{p}'_{T1}$. Plugging in Eq. (5),Eq. (6) andEq. (26) one can see that Eq. (52) takes the form

$$\begin{aligned}&\bar{\alpha}_S^2\int d^2p'_{T1}\frac{1}{p_{T1}^2}\left\{\frac{k_T^2}{k_T'^2}+\frac{l_T^2}{l_T'^2}-\frac{p_{T1}^2}{k_T'^2\,l_T'^2}\right\}\frac{1}{p_{T1}'^2}\left\{\frac{k_T'^2}{k_T''^2}+\frac{l_T'^2}{l_T''^2}-\frac{p_{T1}'^2}{k_T''^2\,l_T''^2}\right\} \\ &\xrightarrow{p'_{T1}\ll k'_T(l'_T)}\;2\,\bar{\alpha}_S^2\int^{k'_T}\frac{d^2p'_{T1}}{p_{T1}'^2}\left[\frac{1}{p_{T1}^2}\left\{\frac{k_T^2}{k_T'^2}+\frac{l_T^2}{l_T'^2}-\frac{p_{T1}^2}{k_T'^2\,l_T'^2}\right\}\right]\;=\;2\,\bar{\alpha}_S^2\int^{\min\{k'_T,l'_T\}}\frac{d^2p'_{T1}}{p_{T1}'^2}\,K\left(\boldsymbol{k}_T-\boldsymbol{l}_T,\boldsymbol{k}_T,\boldsymbol{k}'_T\right)\end{aligned} \tag{53}$$

Note that the term $\Big[\ldots\Big]$ is the same as in Fig. 8 and $K\left(\boldsymbol{k}_T-\boldsymbol{l}_T,\boldsymbol{k}_T,\boldsymbol{k}'_T\right)$ is given by Eq. (26).

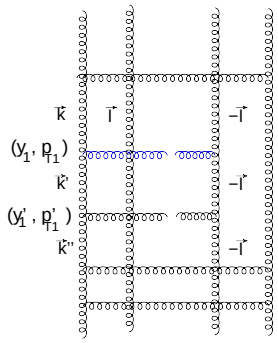

FIG. 16: The part of the diagram of Fig. 15-a with the vertex of emission of two gluons.

Finally, we obtain the following expression for the interference diagram of Fig. 16

$$\begin{aligned}&\frac{d^2\sigma}{dy_1\,dy_2d^2p_{T1}d^2p_{T2}}\left(Fig.\;15-b\right)\;=\;2\left(\frac{2\pi\bar{\alpha}_S}{C_F}\right)^2\bar{\alpha}_S^2\int d^2Q_T G_D\left(Q_T\right)\,G_D\left(\boldsymbol{Q}_T-\boldsymbol{p}_{T,12}\right) \\ &\times\int d^2k_T\;\int d^2l_T\;\phi_G^N\left(Y-y_1;\boldsymbol{k}_T,-\boldsymbol{k}_T\right)\;\phi_G^N\left(Y-y_1;\boldsymbol{l}_T,-\boldsymbol{l}_T\right) \\ &\int^{\min\{k'_T,l'_T\}}\int^{y_1}dy'_1\,\frac{d^2p'_{T1}}{p_{T1}'^2}\,K\left(\boldsymbol{k}_T-\boldsymbol{l}_T,\boldsymbol{k}_T,\boldsymbol{k}'_T\right)\int_{y_2}dy'_2\int^{\min\{q'_T,m'_T\}}\frac{d^2p'_{T2}}{p_{T2}'^2}\,K\left(\boldsymbol{q}_T-\boldsymbol{m}_T,\boldsymbol{q}_T,\boldsymbol{q}'_T\right) \\ &\int d^2q_T\int d^2m_T\,G^{\rm BFKL}\left(y'_1-y'_2;\boldsymbol{p}_{T1};\boldsymbol{k'}_T-\boldsymbol{p}'_{T1},\boldsymbol{q}'_T+\boldsymbol{p}'_{T2}\right)G^{\rm BFKL}\left(y'_1-y'_2;-\boldsymbol{p}_{T1};\boldsymbol{l}'_T-\boldsymbol{p}'_{T1},\boldsymbol{m}'_T+\boldsymbol{p}'_{T2}\right) \\ &\phi_G^N\left(y_2;\boldsymbol{q}_T-\boldsymbol{p}_{T1},-\boldsymbol{q}_T+\boldsymbol{p}_{T2}\right)\,\phi_G^N\left(y_2;\boldsymbol{m}_T,-\boldsymbol{m}_T\right)\end{aligned} \tag{54}$$

In Eq. (54) we put $Q_T=0$ everywhere, except in $G_D\left(Q_T\right)$ and $G_D\left(\boldsymbol{Q}_T-\boldsymbol{p}_{T,12}\right)$, since $Q_T\sim 1/R_D\ll$ all other momenta. At first sight Eq. (54) gives the cross section which is suppressed as $\bar{\alpha}_S^2$ in comparison with Eq. (28). However, the integration over y'_1 and y'_2 leads to $1/\bar{\alpha}_S^2$ contributions, resulting in a cross section of the order of $\bar{\alpha}_S^2$. One can also see, that the cross section does not depend on the rapidity difference y_{12} for the large values of this difference.

The generalization to other cases, which we have considered above, is straightforward, and we not discuss it here.

VI. CONCLUSIONS

A. Comparison with other estimates in perturbative QCD

The first estimate of the azimuthal correlations due to the Bose-Einstein correlation in perturbative QCD, was performed in Ref.[2] (see also Ref.[3]). The diagrams, that were considered in these papers, are shown in Fig. 17-a.

The observation is that these diagrams give rather strong azimuthal correlations, but they are symmetric with respect to $\phi \to \pi - \phi$, and only generate v_n with even n. The general origin of this symmetry was discussed in section II-B for slightly different diagrams. In Refs.[2, 3] the Q_T dependence was neglected leading to δ-function contributions, which were smeared out by Q_T dependance, with $Q_T \sim 1/R$, where R is the size of the interacting dipoles in Fig. 17-a.

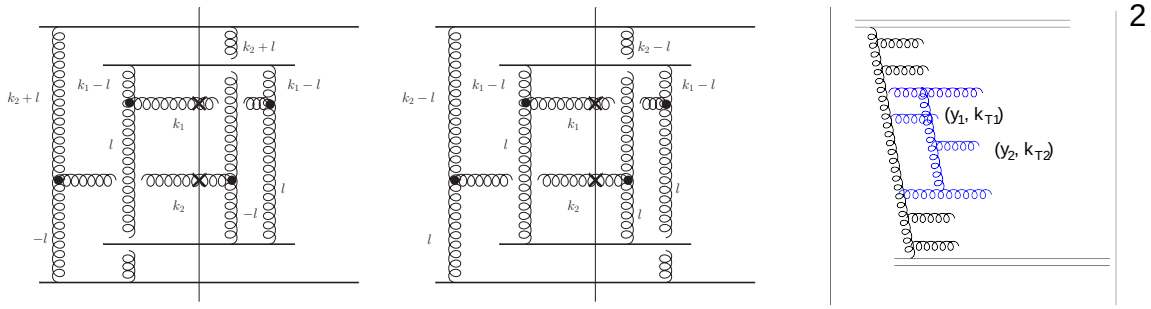

Fig. 17-a Fig. 17-b

FIG. 17: Fig. 17-a is taken from Ref.[2] and describe the correlation in a one parton shower (see Fig. 17-b).

Since Fig. 17-a describes the production of two identical gluons in the dipole-dipole amplitude, in the Born approximation of perturbative QCD, these diagrams are responsible for the azimuthal correlations in one parton cascade shown in Fig. 17-b. It is worthwhile mentioning that the diagram of Fig. 17-a leads to a contribution which is proportional to $\exp\left(-\omega\left(\frac{1}{2},0\right)\, y_{12}\right)$ and describes the correlations that decrease for large y_{12}. Therefore, only for $\omega\left(\frac{1}{2},0\right)\, y_{12} \ll 1$, can we consider this diagram as a source of correlations which are independent of y_{12}.

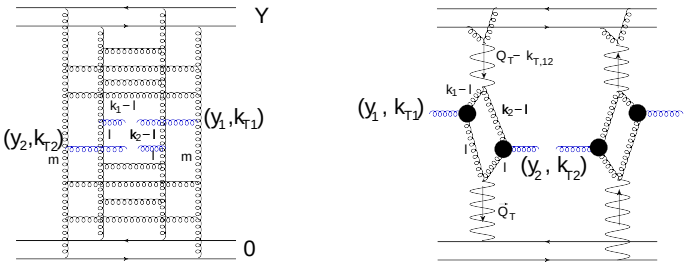

FIG. 18: The generalized diagram of Fig. 17-a, taking into account the gluon emission (two parton shower contribution).

Taking into account the emission of gluons, we can generalize the diagram of Fig. 17-a to the diagram of Fig. 18. We have considered this diagram above, and have shown that there is no symmetry with respect of $\phi \to \pi - \phi$ in such diagrams. Therefore, we conclude that the symmetry $\phi \to \pi - \phi$, is a feature of the azimuthal correlations in the one parton shower, in the Born approximation of perturbative QCD.

B. Summary

In this paper, we found within the framework of perturbative QCD, that the Bose-Einstein correlations due to two parton shower production, induce azimuthal angle correlations, with three correlation lengths: the size of the deuteron, the proton radius, and the size of the BFKL Pomeron which is closely related to the saturation momentum ($R_c \sim 1/Q_s$). These correlations are independent of the values of rapidities of produced gluons (long range rapidity correlations), and have no symmetry with respect to $\phi \to \pi - \phi$ ($\boldsymbol{p}_{T1} \to -\boldsymbol{p}_{T1}$). Therefore, they give rise to v_n for all values of n, not only even values.

We reproduce the result of Refs.[2, 3] which show this symmetry in the Born approximation of perturbative QCD. However, even in the Born approximation, this symmetry depends on the amplitude of the gluon - nucleon interaction at large distances, of about the nucleon size and, therefore, it inherently has a non-perturbative nature. Replacing the nucleon by an onium: the quark-antiquark bound state of heavy quarks, we see that symmetry $\phi \to \pi - \phi$ ($\boldsymbol{p}_{T1} \to -\boldsymbol{p}_{T1}$), does not hold for distances of the order of the size of the onium.

We demonstrated that the azimuthal correlations with the correlation length (R_c) of about the size of the deuteron, and the size of nucleon, stem from a non-perturbative contribution, and their estimates demand a lot of modeling due

to the embryonic state of the theory in the non-perturbative region. However, the correlations with $R_c \sim 1/Q_s$ have a perturbative origin, and can be evaluated in the framework of the Colour Gluon Condensate (CGC) approach.

We show that the two parton showers contributions, generate long range rapidity azimuthal angle correlations, which intuitively have been expected. In other words, we demonstrate that the azimuthal angle correlations do not depend on $y_{12} = |y_1 - y_2|$ for large values of y_{12} ($\bar{\alpha}_S\, y_{12} \geq 1$). We illustrate that the correlation of Refs.[2, 3], actually describe the correlations in a one parton shower, and can be viewed, as independent of the rapidity difference, only in the narrow rapidity window $\bar{\alpha}_S y_{12} \ll 1$.

Acknowledgements We thank our colleagues at Tel Aviv University and UTFSM for encouraging discussions. Our special thanks go to Carlos Cantreras, Alex Kovner and Michel Lublinsky for elucidating discussions on the subject of this paper.

This research was supported by the BSF grant 2012124, by Proyecto Basal FB 0821(Chile) , Fondecyt (Chile) grant 1140842, and by CONICYT grant PIA ACT1406.

Appendix A: Q_T dependence of the BFKL Pomeron

The impact parameter dependence of the BFKL Pomeron is well known[22], and it has the following form for the scattering of two dipoles (r_1 and r_2) at impact parameter b[22, 23]:

$$N_{I\!P}\,(r_1, r_2; Y, b) \;=\; \int \frac{d\gamma}{2\,\pi\,i}\, e^{\omega(\gamma,0)\,Y}\, H^{\gamma}\,(w, w^*) \tag{A1}$$

where

$$\omega(\gamma, 0) \;=\; \bar{\alpha}_S\,(2\psi(1) - \psi(\gamma) - \psi(1-\gamma)) \tag{A2}$$

and where $\psi(z)$ is the Euler $\psi(z) = d\ln\Gamma\,(z)\,/dz$ (digamma function) (see Ref.[31] formula **8.360 - 8.367**).

$$\begin{aligned} H^{\gamma}\,(w, w^*) \qquad &\equiv \qquad \frac{(\gamma - \frac{1}{2})^2}{(\gamma(1-\gamma))^2}\Bigg\{ b_\gamma\, w^{\gamma}\, w^{*\gamma}\, F\,(\gamma, \gamma, 2\gamma, w)\; F\,(\gamma, \gamma, 2\gamma, w^*) \;+ \\ &\qquad\qquad b_{1-\gamma} w^{1-\gamma} w^{*\,1-\gamma} F\,(1-\gamma, 1-\gamma, 2-2\gamma, w)\; F\,(1-\gamma, 1-\gamma, 2-2\gamma, w^*)\Bigg\} \qquad \text{(A3)} \\ &\xrightarrow{w\,w^* \ll 1} \quad \frac{(\gamma - \frac{1}{2})^2}{(\gamma(1-\gamma))^2}\Bigg\{ b_\gamma\, w^{\gamma}\, w^{*\gamma} \;+\; b_{1-\gamma} w^{1-\gamma} w^{*\,1-\gamma}\Bigg\} \qquad \text{(A4)} \end{aligned}$$

where $F \equiv {}_2F_1$ is hypergeometric function [31]. In Eq. (A3) $w\,w^*$ is equal to

$$w\,w^* \;=\; \frac{r_1^2\, r_2^2}{\left(\boldsymbol{b} - \frac{1}{2}\,(\,\boldsymbol{r}_1 \,-\, \boldsymbol{r}_2)\right)^2\,\left(\boldsymbol{b} \,+\, \frac{1}{2}\,(\,\boldsymbol{r}_1 \,-\, \boldsymbol{r}_2)\right)^2} \tag{A5}$$

and b_γ is given by

$$b_\gamma \;=\; \pi^3\, 2^{4(1/2-\gamma)}\, \frac{\Gamma\,(\gamma)}{\Gamma\,(1/2-\gamma)}\, \frac{\Gamma\,(1-\gamma)}{\Gamma\,(1/2+\gamma)}. \tag{A6}$$

From Eq. (A3) and Eq. (A5) we see that (i) b is about of the size of the largest dipole ($b \sim r_2$ for $r_2 \gg r_1$); and (ii) the scattering amplitude has a symmetry with respect to $\boldsymbol{b} \to -\boldsymbol{b}$. Q_T is the conjugated variable to b, since

$$N_{I\!P}\,(r_1, r_2; b; Y) \;=\; r_1^2 r_2^2 \int d^2k\, d^2k' e^{i\boldsymbol{k}_T\cdot\boldsymbol{r}_1 + i\boldsymbol{k'}_T\cdot\boldsymbol{r}_2} \int d^2Q_T\, e^{i\boldsymbol{Q}_T\cdot\boldsymbol{b}}\, G^{\rm BFKL}\,(Y; Q_T; k'_T, k_T) \tag{A7}$$

we see that the value of typical $Q_T \propto 1/r_2 \approx 1/R_N$. In Eq. (A7) $G^{\rm BFKL}\,(y - y'; Q_T; k'_T, k_T)$ denotes the BFKL Pomeron Green's function with the momentum transferred Q_T, and the transverse momenta of gluons k_T at y and k'_T at y'. The initial condition for the BFKL Green's function is the exchange of two gluons at $y = y'$.

In Eq. (A7), the value of r_1 in our problem, is about $1/p_{T1}$ or $1/p_{T2}$, and we trust perturbative QCD calculations only if $p_{T1} \sim p_{T2} \gg 1/R_N$. Since $r_1 \ll r_2$ we can use Eq. (A4) and take $w\,w^*$ to be equal to

$$w\,w^* \;=\; \frac{r_1^2\,r_2^2}{\left(\boldsymbol{b}-\frac{1}{2}\boldsymbol{r}_2\right)^2\,\left(\boldsymbol{b}+\frac{1}{2}\boldsymbol{r}_2\right)^2} \tag{A8}$$

Bearing in mind that

$$I_\gamma\left(\boldsymbol{k}\right) \;=\; \int \frac{d^2r}{\left(r^2\right)^\gamma}\,e^{i\boldsymbol{k}\cdot\boldsymbol{r}} \;=\; 2^{1-2\gamma}\frac{\Gamma\left(1-\gamma\right)}{\Gamma\left(\gamma\right)}\frac{1}{\left(k^2\right)^{1-\gamma}} \tag{A9}$$

Plugging Eq. (A9) in Eq. (A7) we obtain

$$\begin{aligned}
&G^{\rm BFKL}\left(\gamma;\boldsymbol{Q}_T;\boldsymbol{k'}_T,\boldsymbol{k}_T\right) \;=\; \frac{\left(\gamma-\frac{1}{2}\right)^2}{\left(\gamma(1-\gamma)\right)^2}\\
&\times\;\left\{b_\gamma\int d^2m'_T I_{1-\gamma}\left(\boldsymbol{k'}_T-\boldsymbol{m'}_T\right)\,I_\gamma\left(\boldsymbol{m'}-\frac{1}{2}\boldsymbol{Q}_T\right)\,I_\gamma\left(\boldsymbol{m'}+\frac{1}{2}\boldsymbol{Q}_T\right)\,I_{1-\gamma}\left(\boldsymbol{k}_T\right)\right.\\
&+\;\left. b_{1-\gamma}\int d^2m_T I_\gamma\left(\boldsymbol{k'}_T-\boldsymbol{m}_T\right)\,I_{1-\gamma}\left(\boldsymbol{m}-\frac{1}{2}\boldsymbol{Q}_T\right)\,I_{1-\gamma}\left(\boldsymbol{m}+\frac{1}{2}\boldsymbol{Q}_T\right)\,I_\gamma\left(\boldsymbol{k}_T\right)\}\right\}
\end{aligned} \tag{A10}$$

The integrals over m' can be taken by replacing vector variables by the complex coordinates[22]

$$\boldsymbol{k} \;\to\; \rho_k \;=\; k_x \;+\; i\,k_y; \qquad \rho_k^* \;=\; k_x \;-\; i\,k_y; \tag{A11}$$

where k_x and k_y denote the x and y projections of $\boldsymbol{k}$. Using formula **3.197(1)** of Ref.[31] we can take integrals over $d^2m' \;=\; d\rho_{m'}\,d\rho^*_{m'}$:

$$\begin{aligned}
&V_\gamma\left(\boldsymbol{k'_T},\boldsymbol{Q}_T\right) \;=\; \int d^2m'_T I_{1-\gamma}\left(\boldsymbol{k'}_T-\boldsymbol{m'}_T\right)\,I_\gamma\left(\boldsymbol{m'}-\frac{1}{2}\boldsymbol{Q}_T\right)\,I_\gamma\left(\boldsymbol{m'}+\frac{1}{2}\boldsymbol{Q}_T\right) \;=\\
&\int d\rho_{m'}\,d\rho^*_{m'} I_{1-\gamma}\left((\rho_k-\rho_{m'}(\rho_k^*-\rho^*_{m'})\right)\,I_\gamma\left((\rho_{m'}+\frac{1}{2}\rho_Q)(\rho^*_{m'}+\frac{1}{2}\rho^*_Q)\right)\,I_\gamma\left((\rho_{m'}-\frac{1}{2}\rho_Q)(\rho^*_{m'}-\frac{1}{2}\rho^*_Q)\right)\\
&=\; 2^{2-4\gamma}\Gamma^4\left(1-\gamma\right)\,\frac{1}{\left(\left(\boldsymbol{k}_T-\frac{1}{2}\boldsymbol{Q}_T\right)^2\right)^\gamma}\,\frac{1}{\left(Q_T^2\right)^{1-2\gamma}}\,F\left(\gamma,\gamma,1,\frac{\rho_k+\frac{1}{2}\rho_Q}{\rho_k-\frac{1}{2}\rho_Q}\right)\,F\left(\gamma,\gamma,1,\frac{\rho_k^*+\frac{1}{2}\rho_Q^*}{\rho_k^*-\frac{1}{2}\rho_Q^*}\right)
\end{aligned} \tag{A12}$$

$$=\quad\left(\textbf{9.131(1)}\text{ of Ref.[31]}\right)\quad 2^{2-4\gamma}\Gamma^4\left(1-\gamma\right)\frac{1}{\left(Q_T^2\right)^\gamma}\,F\left(\gamma,1-\gamma,1,\frac{\rho_k+\rho_Q}{\rho_Q}\right)\,F\left(\gamma,1-\gamma,1,\frac{\rho_k^*+\rho_Q^*}{\rho_Q^*}\right) \tag{A13}$$

$$=\quad\left(\textbf{9.132(2)}\text{ of Ref.[31]}\right)\quad 2^{2-4\gamma}\Gamma^4\left(1-\gamma\right)\frac{1}{\left(\left(\boldsymbol{k}_T+\boldsymbol{Q}_T\right)^2\right)^\gamma} \tag{A14}$$

$$\begin{aligned}
&\times\left\{\frac{\Gamma\left(1-2\gamma\right)}{\Gamma^2\left(1-\gamma\right)}F\left(\gamma,\gamma,2\gamma,\frac{\rho_Q}{\rho_k+\rho_Q}\right)\;+\;\left(\frac{\rho_Q}{\rho_k+\rho_Q}\right)^{1-2\gamma}\,\frac{\Gamma\left(-1+2\gamma\right)}{\Gamma^2\left(1\gamma\right)}F\left(1-\gamma,1-\gamma,2(1-\gamma),\frac{\rho_Q}{\rho_k+\rho_Q}\right)\right\}\\
&\times\left\{\frac{\Gamma\left(1-2\gamma\right)}{\Gamma^2\left(1-\gamma\right)}F\left(\gamma,\gamma,2\gamma,\frac{\rho_Q^*}{\rho_k^*+\rho_Q^*}\right)\;+\;\left(\frac{\rho_Q^*}{\rho_k^*+\rho_Q^*}\right)^{1-2\gamma}\,\frac{\Gamma\left(-1+2\gamma\right)}{\Gamma^2\left(1\gamma\right)}F\left(1-\gamma,1-\gamma,2(1-\gamma),\frac{\rho*_Q}{\rho_k^*+\rho_Q^*}\right)\right\}
\end{aligned}$$

Plugging Eq. (A11) in Eq. (A10) one can see that $\phi_G^N\left(\gamma,\boldsymbol{k'}_T,\boldsymbol{k}_T,\boldsymbol{Q}_T\right)$ can be written in the factorized form:

$$G^{\rm BFKL}\left(\gamma;\boldsymbol{Q}_T;\boldsymbol{k'}_T,\boldsymbol{k}_T\right) \;=\; V_\gamma\left(\boldsymbol{k'_T},\boldsymbol{Q}_T\right)\,I_\gamma\left(\boldsymbol{k}_T\right)\;+\;V_{1-\gamma}\left(\boldsymbol{k'_T},\boldsymbol{Q}_T\right)\,I_{1-\gamma}\left(\boldsymbol{k}_T\right) \tag{A15}$$

ϕ_G^N in the rapidity representation can be calculated as

$$G^{\rm BFKL}\left(Y;,\boldsymbol{Q}_T;\boldsymbol{k'}_T,\boldsymbol{k}_T\right) \;=\; \int_{\epsilon-i\infty}^{\epsilon+i\infty}\frac{d\gamma}{2\pi i}\,e^{\omega(\gamma,0)Y}\,G^{\rm BFKL}\left(\gamma,\boldsymbol{k'}_T,\boldsymbol{k}_T,\boldsymbol{Q}_T\right) \tag{A16}$$

Taking the integral over γ in Eq. (A16) by the method of steepest descend [18], we see that for large $Y \gg 1$ the essential $\gamma = \frac{1}{2} + i\nu$, where ν is small. Bearing this in mind, we can see from Eq. (A13) that at large $Q_T \gg k'_T$, $G^{\rm BFKL}\left(Y;,\boldsymbol{Q}_T;\boldsymbol{k'}_T,\boldsymbol{k}_T\right) \propto 1/\left(Q_T^2\right)^\gamma \approx 1/Q_T$. At $Q_T \to 0$ $Q_T \gg k'_T$ $G^{\rm BFKL}\left(Y;,\boldsymbol{Q}_T;\boldsymbol{k'}_T,\boldsymbol{k}_T\right) \to$ Const. Therefore, we conclude that the typical value Q_T in the BFKL Pomeron, is about k'_T: the smallest transverse momenta.

At large Y we can simplify Eq. (A16) using Eq. (A15) and the small size of ν. Plugging $G^{\rm BFKL}\left(Y;,\boldsymbol{Q}_T;\boldsymbol{k'}_T,\boldsymbol{k}_T\right)$ from Eq. (A15) in Eq. (A16), we have

$$\begin{aligned} G^{\rm BFKL}\left(Y;\boldsymbol{Q}_T;\boldsymbol{k'}_T,\boldsymbol{k}_T\right) &= \int_{\epsilon-i\infty}^{\epsilon+i\infty}\frac{d\gamma}{2\pi i}\,e^{\omega(\gamma,0)Y}\,2\,V_{\frac{1}{2}+i\nu}\left(\boldsymbol{k'_T},\boldsymbol{Q}_T\right)\,I_\gamma\left(\boldsymbol{k}_T\right) \\ &\xrightarrow{\nu\ll 1} \frac{2\,C\left(\gamma=\frac{1}{2}\right)}{k'_T\,k_T}V_{\frac{1}{2}}\left(\boldsymbol{k'_T},\boldsymbol{Q}_T\right)\int_{-\infty+i\epsilon}^{+\infty+i\epsilon}\frac{d\nu}{2\pi}\,e^{\left(\omega\left(\frac{1}{2},0\right)-D\,\nu^2\right)Y+i\nu\ln\left(k_T^2/k_T'^2\right)} \\ &= \frac{2\,C\left(\gamma=\frac{1}{2}\right)}{k'_T\,k_T}V_{\frac{1}{2}}\left(\boldsymbol{k'_T},\boldsymbol{Q}_T\right)\left(\sqrt{\frac{2\pi}{D\,Y}}\,e^{\omega\left(\frac{1}{2},0\right)Y-\frac{\ln^2\left(k_T'^2/k_T^2\right)}{4\,D\,Y}}\right) \end{aligned} \tag{A17}$$

Integral in Eq. (A17) is taken in the saddle point approximation with $\nu_{SP} = i\ln\left(k_T^2/k_T'^2\right)/2\,DY \ll 1$ and $\omega\left(\frac{1}{2}+i\nu,0\right) = \omega\left(\frac{1}{2},0\right) - D\,\nu^2$.

Appendix B: The BFKL Pomeron - onium vertex

The scattering amplitude of a dipole of size x_{01} with an onium has the following form:

$$A\left(Y,x_{01};Q_T\right) = \int d^2x'_{01}\,e^{i\boldsymbol{x'}_{01}\cdot\boldsymbol{Q}_T}\,\Psi^*_{\rm onium}\left(x'_{01}\right)\,N\left(Y;x'_{01},x_{01},Q_T\right)\,\Psi^*_{\rm onium}\left(x'_{01}\right) \tag{B1}$$

In the momentum representation it can be written as

$$A\left(\gamma,k'_T,k_T,Q_T\right) = \left(F\left(Q_T\right)-F\left(2\boldsymbol{k'}_T-\boldsymbol{Q}_T\right)\right)\int d^2x'_{01}e^{-i\boldsymbol{k'}_T\cdot\boldsymbol{x'}_{01}-i\boldsymbol{k}_T\cdot\boldsymbol{x}_{01}}\,N\left(\gamma;x'_{01},x_{01},Q_T\right)/x_{01}^2 \tag{B2}$$

The amplitude $e^{-i\boldsymbol{k'}_T\cdot\boldsymbol{x'}_{01}-i\boldsymbol{k}_T\cdot\boldsymbol{x}_{01}}\,N\left(\gamma;x'_{01},x_{01},Q_T\right)/x_{01}^2$ can be written in the factorized form of Eq. (A15):

$$e^{-i\boldsymbol{k'}_T\cdot\boldsymbol{x'}_{01}-i\boldsymbol{k}_T\cdot\boldsymbol{x}_{01}}\,N\left(\gamma;x'_{01},x_{01},Q_T\right)/x_{01}^2 = V^{\rm pr}_\gamma\left(\boldsymbol{k'_T},\boldsymbol{Q}_T\right)\,N_\gamma\left(\boldsymbol{k}_T\right) + V^{\rm pr}_{1-\gamma}\left(\boldsymbol{k'_T},\boldsymbol{Q}_T\right)\,N_{1-\gamma}\left(\boldsymbol{k}_T\right) \tag{B3}$$

where $V^{\rm pr}_\gamma\left(\boldsymbol{k'_T},\boldsymbol{Q}_T\right)$ is equal to

$$\begin{aligned} &V^{\rm pr}_\gamma\left(\boldsymbol{k'_T},\boldsymbol{Q}_T\right) = \int d^2m'_T I_{-\gamma}\left(\boldsymbol{k'}_T-\boldsymbol{m'}_T\right)\,I_\gamma\left(\boldsymbol{m'}-\frac{1}{2}\boldsymbol{Q}_T\right)\,I_\gamma\left(\boldsymbol{m'}+\frac{1}{2}\boldsymbol{Q}_T\right) = \\ &\int d\rho_{m'}\,d\rho^*_{m'}I_{-\gamma}\left((\rho_k-\rho_{m'}(\rho^*_k-\rho^*_{m'})\right)\,I_\gamma\left((\rho_{m'}+\frac{1}{2}\rho_Q)(\rho^*_{m'}+\frac{1}{2}\rho^*_Q)\right)\,I_\gamma\left((\rho_{m'}-\frac{1}{2}\rho_Q)(\rho^*_{m'}-\frac{1}{2}\rho^*_Q)\right) \\ &= 2^{3-2\gamma}\frac{\Gamma\left(1+\gamma\right)\Gamma^2\left(1-\gamma\right)}{\Gamma\left(-\gamma\right)\,\Gamma^2\left(\gamma\right)}\,\frac{1}{\left(\left(\boldsymbol{k}_T-\frac{1}{2}\boldsymbol{Q}_T\right)^2\right)^{1+\gamma}}\,\frac{1}{\left(Q_T^2\right)^{1-2\gamma}}\,F\left(1+\gamma,\gamma,2,\frac{\rho_k+\frac{1}{2}\rho_Q}{\rho_k-\frac{1}{2}\rho_Q}\right)\,F\left(1+\gamma,\gamma,2,\frac{\rho^*_k+\frac{1}{2}\rho^*_Q}{\rho^*_k-\frac{1}{2}\rho^*_Q}\right) \end{aligned} \tag{B4}$$

Finally, the BFKL Pomeron-onium vertex takes the form

$$V^{\rm onium}_\gamma\left(Q_T\right) = \int d^2k'_T\left(F\left(Q_T\right)-F\left(2\boldsymbol{k'}_T-\boldsymbol{Q}_T\right)\right)\,V^{\rm pr}_\gamma\left(\boldsymbol{k'_T},\boldsymbol{Q}_T\right) \tag{B5}$$

* Electronic address: gotsman@post.tau.ac.il
† Electronic address: leving@post.tau.ac.il, eugeny.levin@usm.cl

[1] E. M. Levin, M. G. Ryskin and S. I. Troian, Sov. J. Nucl. Phys. **23** (1976) 222 [Yad. Fiz. **23** (1976) 423]; A. Capella, A. Krzywicki and E. M. Levin, Phys. Rev. D **44** (1991) 704.
[2] Y. V. Kovchegov and D. E. Wertepny, Nucl. Phys. A **906** (2013) 50, [arXiv:1212.1195 [hep-ph]];

[3] T. Altinoluk, N. Armesto, G. Beuf, A. Kovner and M. Lublinsky, Phys. Lett. B **752** (2016) 113, [arXiv:1509.03223 [hep-ph]]; T. Altinoluk, N. Armesto, G. Beuf, A. Kovner and M. Lublinsky, Phys. Lett. B **751** (2015) 448, [arXiv:1503.07126 [hep-ph]].

[4] E. Gotsman, E. Levin and U. Maor, *"Bose-Einstein correlations and* $\mathbf{v_{2n}}$ *and* $\mathbf{v_{2n-1}}$ *in hadron and nucleus collisions,"* arXiv:1604.04461 [hep-ph]; *"CGC/saturation approach for high energy soft interactions: 'soft' Pomeron structure and* v_n *in hadron and nucleus collisions from Bose-Einstein correlation,"* arXiv:1607.00594 [hep-ph].

[5] V. Khachatryan *et al.* [CMS Collaboration], arXiv:1510.03068 [nucl-ex]; JHEP **1009** (2010) 091 [arXiv:1009.4122 [hep-ex]]. arXiv:1510.03068 [nucl-ex].

[6] J. Adams *et al.* [STAR Collaboration], Phys. Rev. Lett. **95** (2005) 152301 [nucl-ex/0501016].

[7] B. Alver *et al.* [PHOBOS Collaboration], Phys. Rev. Lett. **104** (2010) 062301 [arXiv:0903.2811 [nucl-ex]].

[8] H. Agakishiev *et al.* [STAR Collaboration], arXiv:1010.0690 [nucl-ex].

[9] S. Chatrchyan *et al.* [CMS Collaboration], Phys. Lett. B **718** (2013) 795 [arXiv:1210.5482 [nucl-ex]]; V. Khachatryan *et al.* [CMS Collaboration], JHEP **1009** (2010) 091, [arXiv:1009.4122 [hep-ex]].

[10] S. Chatrchyan *et al.* [CMS Collaboration], JHEP **1402** (2014) 088, [arXiv:1312.1845 [nucl-ex]]; Phys. Rev. C **89** (2014) no.4, 044906; [arXiv:1310.8651 [nucl-ex]]; "Centrality dependence of dihadron correlations and azimuthal anisotropy harmonics in PbPb collisions at $\sqrt{s_{NN}} = 2.76$ TeV," Eur. Phys. J. C **72** (2012) 2012 [arXiv:1201.3158 [nucl-ex]]; JHEP **1402** (2014) 088 doi:10.1007/JHEP02(2014)088 [arXiv:1312.1845 [nucl-ex]].

[11] J. Adam *et al.* [ALICE Collaboration], arXiv:1604.07663 [nucl-ex]; Phys. Rev. Lett. **116** (2016) no.13, 132302 doi:10.1103/PhysRevLett.116.132302 [arXiv:1602.01119 [nucl-ex]]; L. Milano [ALICE Collaboration], Nucl. Phys. A **931** (2014) 1017, [arXiv:1407.5808 [hep-ex]]; Y. Zhou [ALICE Collaboration], J. Phys. Conf. Ser. **509** (2014) 012029, [arXiv:1309.3237 [nucl-ex]].

[12] B. B. Abelev *et al.* [ALICE Collaboration], Phys. Rev. C **90** (2014) no.5, 054901, [arXiv:1406.2474 [nucl-ex]]; B. B. Abelev *et al.* [ALICE Collaboration], Phys. Lett. B **726** (2013) 164 doi:10.1016/j.physletb.2013.08.024 [arXiv:1307.3237 [nucl-ex]]; B. Abelev *et al.* [ALICE Collaboration], Phys. Lett. B **719** (2013) 29, [arXiv:1212.2001 [nucl-ex]].

[13] G. Aad *et al.* [ATLAS Collaboration], Phys. Rev. Lett. **116** (2016) 172301, [arXiv:1509.04776 [hep-ex]].

[14] G. Aad *et al.* [ATLAS Collaboration], Phys. Rev. C **90** (2014) no.4, 044906; [arXiv:1409.1792 [hep-ex]]; B. Wosiek [ATLAS Collaboration], Annals Phys. **352** (2015) 117; G. Aad *et al.* [ATLAS Collaboration], Phys. Lett. B **725** (2013) 60, [arXiv:1303.2084 [hep-ex]].

[15] B. Wosiek [ATLAS Collaboration], Phys. Rev. C **86** (2012) 014907, [arXiv:1203.3087 [hep-ex]].

[16] R. Hanbury Brown and R. Q. Twiss, Nature **178** (1956) 1046.

[17] G. Goldhaber, W. B. Fowler, S. Goldhaber and T. F. Hoang, Phys. Rev. Lett. **3**, 181 (1959); G. I. Kopylov and M. I. Podgoretsky, Sov. J. Nucl. Phys. **15**, 219 (1972) [Yad. Fiz. **15**, 392 (1972)]; G. Alexander, Rept. Prog. Phys. **66** (2003) 481, [hep-ph/0302130].

[18] Yuri V Kovchegov and Eugene Levin, *" Quantum Choromodynamics at High Energies"*, Cambridge Monographs on Particle Physics, Nuclear Physics and Cosmology, Cambridge University Press, 2012 .

[19] R.J. Glauber, In: Lectures in Theor. Phys., v. 1, ed. W.E. Brittin and L.G. Duham. NY: Intersciences, 1959

[20] V. A. Abramovsky, V. N. Gribov and O. V. Kancheli, Yad. Fiz. **18**, 595 (1973) [Sov. J. Nucl. Phys. **18**, 308 (1974)].

[21] E. A. Kuraev, L. N. Lipatov, and F. S. Fadin, *Sov. Phys. JETP* **45**, 199 (1977); Ya. Ya. Balitsky and L. N. Lipatov, *Sov. J. Nucl. Phys.* **28**, 22 (1978).

[22] L. N. Lipatov, Phys. Rep. **286** (1997) 131; Sov. Phys. JETP **63** (1986) 904 and references therein.

[23] H. Navelet and R. B. Peschanski, Nucl. Phys. **B 507**, 35 (1997) [hep-ph/9703238]; Phys. Rev. Lett. **82** (1999) 1370 [hep-ph/9809474]; Nucl. Phys. B **634** (2002) 291 [hep-ph/0201285].

[24] E. Levin and A. H. Rezaeian, Phys. Rev. D **84** (2011) 034031, [arXiv:1105.3275 [hep-ph]].

[25] E. Gotsman, E. Levin, U. Maor and S. Tapia, Phys. Rev. D **93** (2016) no.7, 074029, [arXiv:1603.02143 [hep-ph]].

[26] V. N. Gribov, Sov. Phys. JETP **26** (1968) 414 [Zh. Eksp. Teor. Fiz. **53** (1967) 654].

[27] L. V. Gribov, E. M. Levin and M. G. Ryskin, Phys. Rep. **100** (1983) 1.

[28] A. H. Mueller, *Phys. Rev.* **D2** (1970) 2963.

[29] M. A. Braun, Phys. Lett. B **632** (2006) 297, [Eur. Phys. J. C **48** (2006) 511] [hep-ph/0512057]; *"Conformal invariant equations for nucleus-nucleus scattering in perturbative QCD with N(c) to infinity,"* hep-ph/0504002; Eur. Phys. J. C **16** (2000) 337 [hep-ph/0001268].

[30] M. Kozlov, E. Levin and A. Prygarin, Nucl. Phys. A **792** (2007) 122, [arXiv:0704.2124 [hep-ph]].

[31] I. Gradstein and I. Ryzhik, *Table of Integrals, Series, and Products*, Fifth Edition, Academic Press, London, 1994.

[32] F. Ferro [TOTEM Collaboration], AIP Conf. Proc. **1350**, 172 (2011) ; G. Antchev *et al.* [TOTEM Collaboration], Europhys. Lett. **96**, 21002 (2011), **95**, 41001 (2011) [arXiv:1110.1385 [hep-ex]]; G. Antchev *et al.* [TOTEM Collaboration], Phys. Rev. Lett. **111** (2013) 26, 262001 [arXiv:1308.6722 [hep-ex]].

[33] E. Gotsman, E. Levin and U. Maor, Eur. Phys. J. C **75** (2015) 5, 179 [arXiv:1502.05202 [hep-ph]]; Eur. Phys. J. C **75** (2015) 1, 18 [arXiv:1408.3811 [hep-ph]]; Phys. Lett. B **746** (2015) 154 [arXiv:1503.04294 [hep-ph]]; . Eur. Phys. J. C **75** (2015) 11, 518 [arXiv:1508.04236 [hep-ph]].

[34] I. Balitsky, [arXiv:hep-ph/9509348]; *Phys. Rev.* **D60**, 014020 (1999) [arXiv:hep-ph/9812311]; Y. V. Kovchegov, *Phys. Rev.* **D60**, 034008 (1999), [arXiv:hep-ph/9901281].

[35] J. Jalilian-Marian, A. Kovner, A. Leonidov and H. Weigert, *Phys. Rev.* **D59**, 014014 (1999), [arXiv:hep-ph/9706377]; *Nucl. Phys.* **B504**, 415 (1997), [arXiv:hep-ph/9701284]; J. Jalilian-Marian, A. Kovner and H. Weigert, *Phys. Rev.* **D59**, 014015 (1999), [arXiv:hep-ph/9709432]; A. Kovner, J. G. Milhano and H. Weigert, *Phys. Rev.* **D62**, 114005 (2000), [arXiv:hep-ph/0004014] ; E. Iancu, A. Leonidov and L. D. McLerran, *Phys. Lett.* **B510**, 133 (2001);

[arXiv:hep-ph/0102009]; *Nucl. Phys.* **A692**, 583 (2001), [arXiv:hep-ph/0011241]; E. Ferreiro, E. Iancu, A. Leonidov and L. McLerran, *Nucl. Phys.* **A703**, 489 (2002), [arXiv:hep-ph/0109115]; H. Weigert, *Nucl. Phys.* **A703**, 823 (2002), [arXiv:hep-ph/0004044].

[36] Y. M. Shabelski and A. G. Shuvaev, Eur. Phys. J. C **75** (2015) no.9, 438, [arXiv:1504.03499 [hep-ph]]; JHEP **1411** (2014) 023, [arXiv:1406.1421 [hep-ph]]; S. Bondarenko and E. Levin, Eur. Phys. J. C **51** (2007) 65, [hep-ph/0511124]; S. Bondarenko, E. Levin and J. Nyiri, Eur. Phys. J. C **25** (2002) 277, [hep-ph/0204156]; J.J.J. Kokkedee, *" The Quark Model"*, NY, W.A. Benjamin, 1969 and references therein; H. J. Lipkin and F. Scheck, Phys. Rev. Lett. **16** (1966) 71; E. M. Levin and L. L. Frankfurt, JETP Lett. **2** (1965) 65.